1521-009X/50/1/65–75$35.00
DRUG METABOLISM AND DISPOSITION


https://doi.org/10.1124/dmd.121.000563
Drug Metab Dispos 50:65–75, January 2022



*Minireview*

# Addressing Today's Absorption, Distribution, Metabolism, and Excretion (ADME) Challenges in the Translation of In Vitro ADME Characteristics to Humans: A Case Study of the *SMN2* mRNA Splicing Modifier Risdiplam[S]

Stephen Fowler[1], Andreas Brink[1], Yumi Cleary, Andreas Günther, Katja Heinig, Christophe Husser, Heidemarie Kletzl, Nicole Kratochwil, Lutz Mueller, Mark Savage, Cordula Stillhart, Dietrich Tuerck, Mohammed Ullah, Kenichi Umehara, and Agnès Poirier

*Pharmaceutical Sciences, Roche Pharma Research and Early Development, Roche Innovation Center Basel (S.F., A.B., Y.C., A.G., K.H., C.H., H.K, N.K., L.M., D.T., M.U., K.U., A.P.) and Formulation & Process Sciences, Pharmaceutical Research and Development (C.S.), F. Hoffmann-La Roche Ltd., Basel, Switzerland; and Unilabs York Bioanalytical Solutions, Sandwich, United Kingdom (M.S.)*

Received June 3, 2021; accepted September 30, 2021

## ABSTRACT

**Small molecules that present complex absorption, distribution, metabolism, and elimination (ADME) properties can be challenging to investigate as potential therapeutics. Acquiring data through standard methods can yield results that are insufficient to describe the in vivo situation, which can affect downstream development decisions. Implementing in vitro–in vivo–in silico strategies throughout the drug development process is effective in identifying and mitigating risks while speeding up their development. Risdiplam (Evrysdi)—an orally bioavailable, small molecule approved by the US Food and Drug Administration and more recently by the European Medicines Agency for the treatment of patients ≥2 months of age with spinal muscular atrophy—is presented here as a case study. Risdiplam is a low-turnover compound whose metabolism is mediated through a non–cytochrome P450 enzymatic pathway. Four main challenges of risdiplam are discussed: predicting in vivo hepatic clearance, determining in vitro metabolites with regard to metabolites in safety testing guidelines, elucidating enzymes responsible for clearance, and estimating potential drug-drug interactions. A combination of in vitro and in vivo results was successfully extrapolated and used to develop a robust physiologically based pharmacokinetic model of risdiplam. These results were verified through early clinical studies, further strengthening the understanding of the ADME properties of risdiplam in humans. These approaches can be applied to other compounds with similar ADME profiles, which may be difficult to investigate using standard methods.**

## SIGNIFICANCE STATEMENT

**Risdiplam is the first approved, small-molecule, *survival of motor neuron 2* mRNA splicing modifier for the treatment of spinal muscular atrophy. The approach taken to characterize the absorption, distribution, metabolism, and excretion (ADME) properties of risdiplam during clinical development incorporated in vitro–in vivo–in silico techniques, which may be applicable to other small molecules with challenging ADME. These strategies may be useful in improving the speed at which future drug molecules can be developed.**



This work was supported by F. Hoffmann-La Roche.

S.F., A.G., K.U., K.H., and N.K. are employees and A.B., Y.C., C.H., H.K., L.M., A.P., and C.S. are employees and shareholders of F. Hoffmann-La Roche Ltd. D.T. is an employee and shareholder of F. Hoffmann-La Roche AG. M.U. was an employee of F. Hoffmann-La Roche at the time of the study. M.S. is an employee of Unilabs York Bioanalytical Solutions and was commissioned and paid by F. Hoffmann-La Roche to perform metabolism and drug metabolism and pharmacokinetics studies.

[1]S.F. and A.B. contributed equally to this work.

dx.doi.org/10.1124/dmd.121.000563.

[S] This article has supplemental material available at dmd.aspetjournals.org.

## Introduction

The preclinical investigation of drug candidates is an important step in the drug development process which enables the selection of the most promising molecule and predicts their likely pharmacokinetics in humans. This stage provides valuable information on the likely safety and tolerability of a drug candidate before entering clinical trials. Assessing the pharmacokinetic (PK) properties, polymorphism risks, and drug-drug interaction (DDI) potential of a new drug requires a considerable number of in vitro and in vivo preclinical studies over an

**ABBREVIATIONS:** ADME, absorption, distribution, metabolism, and excretion; AUC, area under the concentration-time curve; $AUC_{inf}$, area under the curve extrapolated to infinity; $AUC_{0\text{-}48}$, area under the plasma concentration-time curve from time 0 to 48 hours; BCRP, breast cancer resistance protein; DDI, drug-drug interaction; DME, drug-metabolizing enzyme; ER, efflux ratio; FDA, US Food and Drug Administration; $f_m$, fraction metabolized; FMO, flavin-containing monooxygenase; hADME, human radiolabeled ADME; HH, human hepatocyte; HLM, human liver microsome; HV, healthy volunteer; [I], inhibitor concentration; $K_I$, inhibitory constant; MATE, multidrug and toxin extrusion protein; MDR1, multidrug resistance mutation; MIST, metabolites in safety testing; MS, mass spectrometry; OCT2, organic cation transporter 2; P450, cytochrome P450; PBPK, physiologically based PK; PK, pharmacokinetic; SAD, single ascending dose; SMA, spinal muscular atrophy; SMN, survival of motor neuron; TDI, time-dependent inhibition.

extended time. However, for compounds with challenging absorption, distribution, metabolism, and excretion (ADME) properties (e.g., low turnover, metabolism by enzymes that are not well understood, and generation of a complex profile of metabolites), the extrapolation of in vitro data to humans cannot be performed with high confidence. This is especially the case when traditional in vitro systems [e.g., human liver microsomes (HLMs) and human hepatocyte (HH) suspensions] may not be sufficiently sensitive for prediction of PK parameters, such as clearance. In such situations, a combination of in vitro experimentation, model-based prediction, and in vivo confirmation is needed to build up a combined description of drug metabolism and pharmacokinetics (Cleary et al., 2018).

Modeling and simulation-based approaches are now included in all areas of preclinical drug development programs, particularly physiologically based PK (PBPK) modeling (Jones and Rowland-Yeo, 2013). Through a "bottom up" approach, PBPK models input data from in vitro assays with human cells and preclinical animal studies to understand the mechanism of a drug's absorption and disposition. When in vitro data coupled with in silico data are sufficiently reliable, PBPK-derived simulations can speed up molecule development by assisting in designing the most informative clinical studies and providing model-based predictions in lieu of others (Fowler et al., 2017). Moreover, PBPK models can extrapolate pharmacokinetics across different populations and disease states, which are used to inform clinical trials, dose-escalation studies, and possible DDIs (Jones and Rowland-Yeo, 2013). More notably, PBPK models have been used to develop prescribing labels (e.g., DDIs) and are now accepted as part of the clinical pharmacology regulatory applications submitted to the US Food and Drug Administration (FDA) (Zhang et al., 2020).

Risdiplam (Evrysdi), a recently approved drug with a challenging ADME profile (US Food and Drug Administration, 2020c; European Medicines Agency, 2021), serves as a case study for an ADME strategy used to inform clinical development. Risdiplam is an orally available small molecule for the treatment of spinal muscular atrophy (SMA). SMA is an autosomal recessive neuromuscular disease caused by deletions and mutations of the *survival of motor neuron (SMN) 1* gene, which result in reduced levels of functional SMN protein. A second *SMN* gene, *SMN2*, produces only low levels of functional SMN protein, which are insufficient to fully compensate for the lack of the *SMN1* gene (Lorson et al., 1999). This results in a progressive loss of spinal motor neurons leading to muscle atrophy and disease-related complications affecting the whole body (Yeo and Darras, 2020) and may be diagnosed in infancy, childhood (types 1–3), or adulthood (type 4) (Mercuri et al., 2020). Risdiplam acts by modifying *SMN2* mRNA splicing, ensuring that more full-length transcripts are generated, and thus increasing SMN protein levels (Ratni et al., 2018). It is to be expected that molecules with new chemical characteristics may be required to address such novel drug-targeting mechanisms and that ADME scientists will need to learn about how best to translate the drug properties of these new compounds into in vivo situations.

Herein we describe some of the challenges met and advances made while translating the ADME characteristics of an mRNA splicing modifying drug to the in vivo environment. By doing so, we further report new data on the safety and PK profile of risdiplam. Comprehensive methodological information and additional supporting data are available in the Supplemental Materials. Four main areas will be examined as shown in Fig. 1: 1) predicting in vivo hepatic clearance from low in vitro turnover, 2) determining in vitro metabolites that are relevant in humans [with regard to metabolites in safety testing (MIST) guidelines], 3) elucidating enzymes responsible for hepatic and extrahepatic clearance, and 4) estimating potential DDIs. The work describes challenges encountered in the modern drug discovery setting and highlights strategies that could be adopted to ensure better predictions for future drug compounds.

## Metabolic Clearance Prediction for Risdiplam, a Low-Clearance Compound

Predicting clearance of drug candidates as accurately as possible is important in drug optimization because it shapes several aspects of pharmacokinetics, including the oral bioavailability, half-life, and effective dose. Risdiplam was optimized toward low intrinsic clearance and avoidance of issues observed in previous drug candidates [e.g., high levels of active metabolite (Ratni et al., 2018)] by making use of HH suspension cultures as an assay system. HHs are the system of choice for optimizing metabolism-based clearance because they have a full complement of drug-metabolizing enzymes (DMEs) (Hutzler et al., 2015) and are available as high-quality cryopreserved preparations from multiple pooled donors, which represent a "population average." However, these primary cells lose function over a time span of ∼4–6 hours (Hutzler et al., 2015), and the lower limit of intrinsic clearance measurement is only ∼3 μl/min per million cells in suspension culture (Docci et al., 2019).

Recently, considerable effort has been invested by many laboratories into validating novel in vitro systems for low-clearance measurements. In the case of risdiplam, the parent drug remained largely unmetabolized after incubation in HLMs (89% remaining after 1 hour) and hepatocytes (98% remaining after 3 hours) with an intrinsic clearance <3 μl/min per million cells. A more advanced in vitro system was therefore needed for accurate intrinsic clearance determination. HepatoPac was chosen because it offered pooled donor hepatocyte cultures, high reproducibility of intrinsic clearance determinations between experiments, and thorough in-house validation (Kratochwil et al., 2017; Docci et al., 2020; Umehara et al., 2020) in which it improved the accuracy and precision of hepatic intrinsic metabolic clearance predictions compared with hepatocytes in monoculture. HepatoPac is a well established, long-term HH coculture system that can maintain viability and functional expression of DMEs for up to 7 days (Khetani and Bhatia, 2008; Underhill and Khetani, 2018). In addition, reduced error in the in vivo intrinsic clearance prediction was observed using the HepatoPac system when compared with hepatocytes in suspension culture (Umehara et al., 2020). The HepatoPac long-term incubation system substantially lowers the intrinsic clearance quantification limit to 0.1–0.3 μl/min per million cells (Da-Silva et al., 2018; Docci et al., 2019; Umehara et al., 2020), and this improved sensitivity enabled risdiplam intrinsic clearance of 0.7 μl/min per million cells to be determined. These data were then scaled to predict the in vivo clearance, the result of which was in excellent agreement (34% higher) with that observed in vivo. To our knowledge, risdiplam is the first drug to come to the market for which advanced long-term hepatocyte cocultures were used prospectively for intrinsic clearance measurement and scaling to in vivo conditions.

## Low In Vitro Turnover of Risdiplam Warranted Early Confirmation of MIST-Relevant Metabolites in Human Plasma Samples

According to MIST guidance, drug metabolites present at >10% of total drug-related exposure at steady state in humans are a potential safety concern (US Food and Drug Administration, 2016). Such metabolites need to be characterized in greater depth (e.g., ADME parameters or target activity) and included in the pharmacology and safety assessment (e.g., via demonstration of exposure coverage in animal toxicity

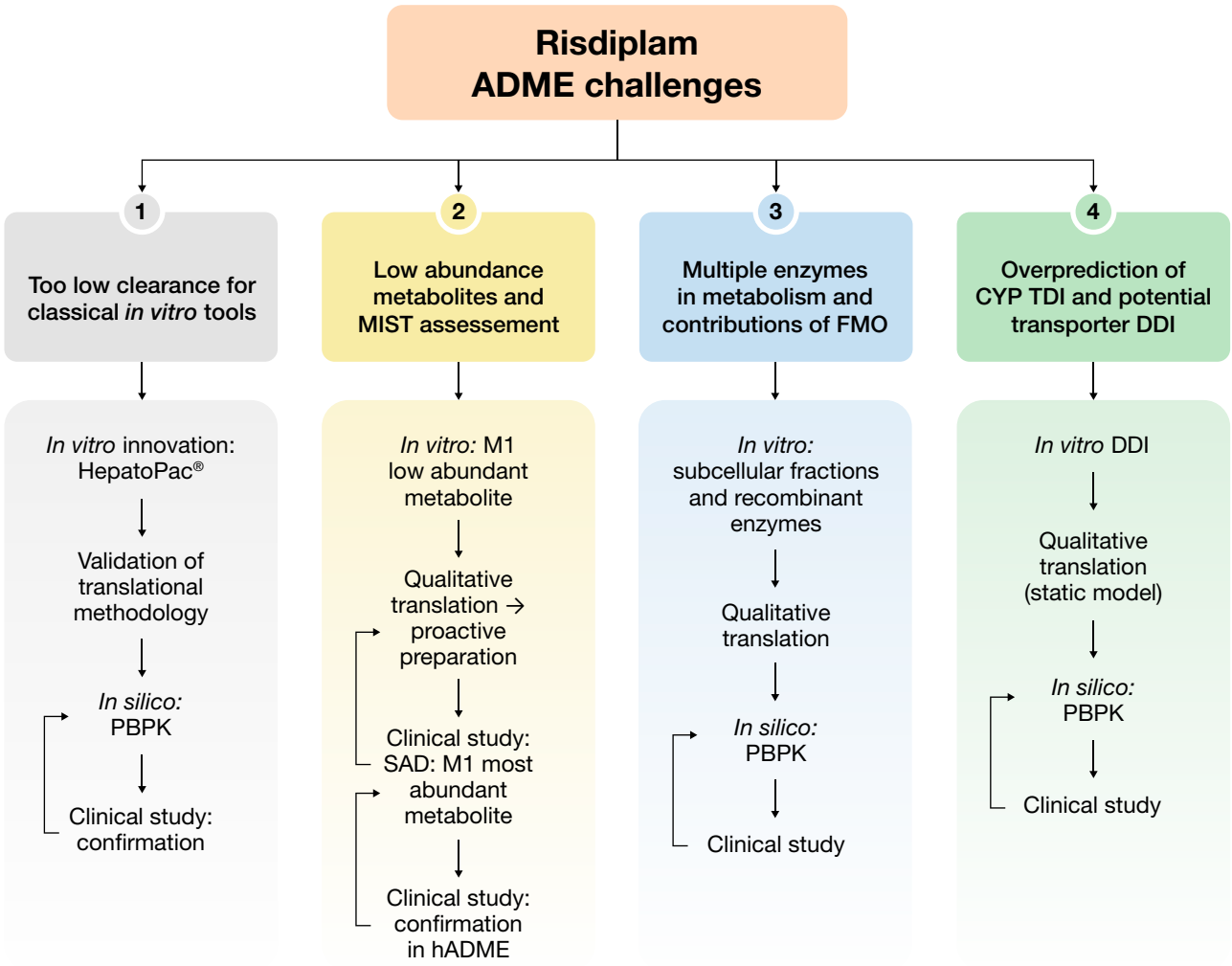


**Fig. 1.** Four main challenges of risdiplam. ADME, absorption, distribution, metabolism, and excretion; CYP, cytochrome P450; DDI, drug-drug interaction; FMO, flavin-containing monooxygenase; hADME, human radiolabeled ADME; MIST, metabolites in safety testing; PBPK, physiologically-based pharmacokinetic; SAD, single ascending dose; TDI, time-dependent inhibition.

studies). Hepatocytes (and other subcellular fractions) provide a view of the principal metabolites and metabolic pathways for most compounds. However, because of multiple (and difficult to assess) parameters in vivo, determining which metabolite(s) would circulate—and can also reach or exceed 10% of the total drug-related material in plasma—is not easily predictable solely with in vitro data (US Food and Drug Administration, 2016; Schadt et al., 2018).

Risdiplam showed only low turnover in incubations with HLMs (11% in 1 hour) and HHs (2% after 3 hours). Consequently, risdiplam produced metabolites at low mass spectrometry (MS) signal intensities in liver microsomes and even lower signal intensities in hepatocytes. Although the *N*-hydroxyl M1 was the most abundant metabolite, the mass spectrum peak intensities were measured in low percentages of total drug-related MS signal intensities (1.7% in hepatocytes and 3.8% in microsomes after 3 hours; Fig. 2A). Other oxidative metabolites (M2–M8) were present at even smaller peak intensities or seen at trace levels (M2–M8).

From a single-ascending-dose (SAD) study [18 mg of risdiplam (Sturm et al., 2019)] in healthy volunteers (HVs; NCT02633709), the plasma metabolite profile was assessed using pooled plasma samples (cross-subject pools of individual time points), which revealed that the main components were parent drug and the *N*-hydroxyl metabolite M1 (Fig. 2; Supplemental Fig. 1). It also found that M1 exceeded 10% of the total drug-related MS signal intensities, which triggered additional bioanalytical method development for M1. Further exploration of M1 showed that it was devoid of any significant primary (*SMN2* splicing) or secondary (*FOXM1* splicing) pharmacological activity at therapeutic doses of risdiplam (Ratni et al., 2018).

After the SAD study, a human radiolabeled ADME (hADME) study (oral administration of $^{14}$C-risdiplam to HVs, NCT03036501) was conducted to identify circulating metabolites in plasma samples collected up to 48 hours postdose. Figures 2B and 3 show the plasma-time profile for total radioactivity, risdiplam, and its metabolites, which confirmed that risdiplam was the major drug-related component found in circulation and M1 was a major circulating metabolite exceeding 10% of total drug-related material. Four additional low-level metabolites (M2, M7, M9, and M26) from biotransformation of the piperazine moiety were observed in plasma. No individual metabolite accounted for more than 2.2% relative to the area under the concentration-time curve (AUC) of total drug-related material in plasma. All other circulating metabolites were below the limit of detection of the metabolite identification radioprofiling method used in the [$^{14}$C]-hADME study. For additional results, see Supplemental Fig. 2–4 and Supplemental Table 1.

The metabolism of risdiplam illustrates the challenges drug metabolism scientists face predicting the relevance of human in vivo

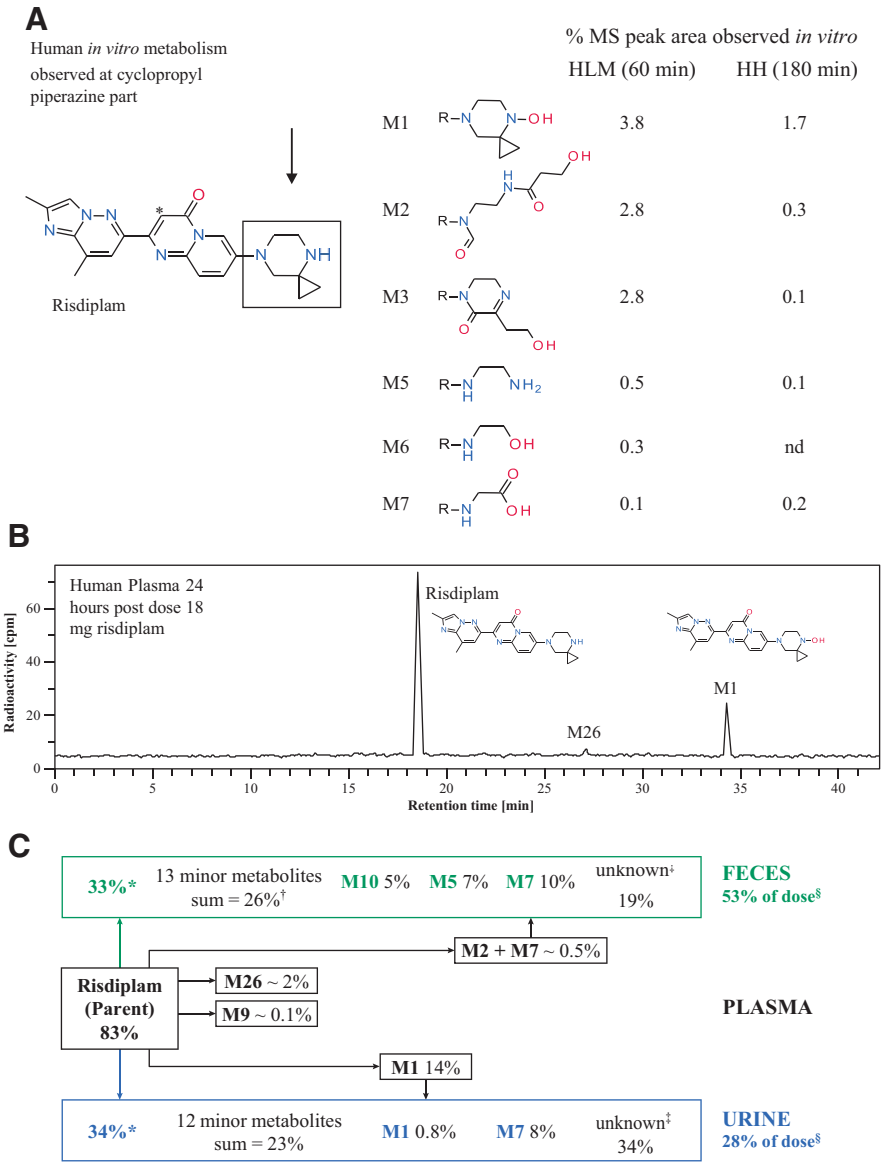


**Fig. 2.** Overview of risdiplam disposition metabolism and excretion in humans after a single oral dose of 18 mg. (A) In vitro metabolites identified in incubations of HLMs and HHs after 60 and 180 minutes, respectively. (B) High-performance liquid chromatography and microbeta-scintillation count analysis of the metabolite profile of risdiplam in pooled human plasma of six healthy individuals at 24 hours after oral administration (18 mg) of [$^{14}$C]-risdiplam. (C) Overview of risdiplam disposition, metabolism, and excretion after a single oral dose of 18 mg in six heathy volunteers. An asterisk on the structure of risdiplam denotes the carbon-14 labeling position in the molecules. Unit (plasma, feces, and urine): percentage of total drug-related material (radioactivity) in the given matrix (of $AUC_{0\text{-}48}$ in plasma and over 0–168 hours in excreta). Approximately 14% and 17% of orally administered 18 mg of [$^{14}$C]-risdiplam was recovered as unchanged in the pooled feces collected over 168 and 840 hours, respectively. *Percent radioactivity recovered after 0–168 hours. †Individual contributions: 0.2%–3.5% of drug-related material in feces (cumulated = 9.6% of the dose) and 0.4%–4.5% of drug-related material in urine (cumulated = 5.3% of the dose). ‡Trace-level components each accounting for <0.9% of the dose (feces) or ≤1.0% of the dose (urine). §Recovered dose after 0–840 hours. $AUC_{0\text{-}48}$, area under the plasma concentration−time curve from time 0 to 48 hours; HH, human hepatocyte; HLM, human liver microsome; MS, mass spectrometry.

metabolites from in vitro incubations of low-turnover compounds. The in vitro metabolic profile was comprised of numerous low-level metabolites, and the quantitative translation from in vitro to in vivo was poor. The profile that was finally observed in plasma circulation was mainly risdiplam and M1 (with M1 exceeding 10% of total drug-related material). For low-turnover compounds, such as risdiplam, in vitro systems are limited in accurately anticipating the extent to which metabolites will circulate in vivo as distribution and excretion of metabolites is not reflected in vitro. However, qualitatively, the principal metabolic biotransformation pathways were well reflected in vitro, and the data could be used to inform potential frontloading activities (e.g., structure elucidation by nuclear magnetic resonance for lower-level metabolites). Therefore, in vitro profiles were still of key importance to mitigate the risk of discovering disproportionate metabolites (according to MIST guidance) late in development, despite not being quantitatively predictive.

**Major Metabolite (M1) Coverage in Plasma of Nonclinical Species** The major metabolite M1 was detected in mouse, rat, rabbit, and monkey plasma. The nonclinical coverage of M1 in pivotal nonclinical studies at the respective no observed adverse effect level for these species is summarized in Table 1. Coverage was assessed based on the median M1/parent ratio (0.334) in patients with SMA at steady state at pivotal doses.

**Metabolite Identification at Later Time Points and Implications for Regulatory Approval of Risdiplam** In plasma samples from the [$^{14}$C]-hADME study, metabolites were identified using a radioprofiling method up to 48 hours postdose because radioactivity levels dropped below the sensitivity of the radioprofiling method used. However, some metabolites may have longer plasma half-lives compared with the parent compound, which would indicate slower elimination rates limiting their clearance (Holmberg et al., 2014). Uncertainties about the levels of metabolites at later time points can be a concern because of potential accumulation after repeated doses, and this was raised during a Health Authority assessment of risdiplam. The Health Authority assessment questioned whether the truncated area under the plasma concentration-time curve from time 0–48 hours ($AUC_{0\text{-}48h}$) was representative of AUC extrapolated to infinity, and therefore, an investigation was conducted to identify any persistent major metabolites.

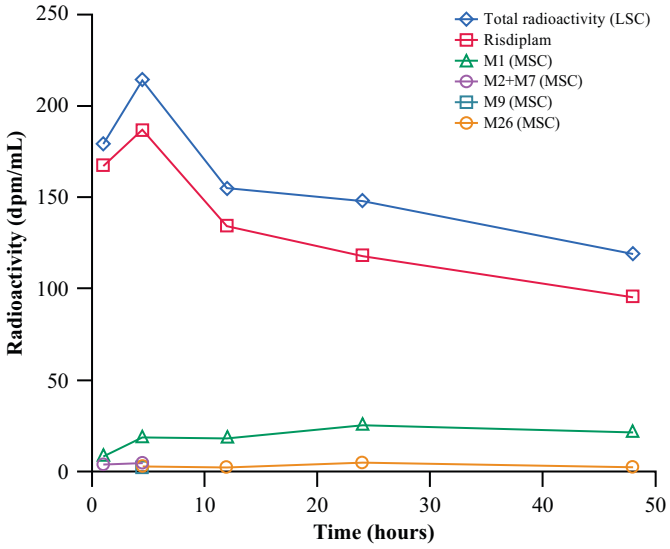


**Fig. 3.** Plasma-time profile for total radioactivity, risdiplam, and its metabolites M1, M2, M7, M9, and M26 in human plasma after oral administration (18 mg) of [$^{14}$C]-risdiplam. LSC, liquid scintillation counting; MSC, microplate scintillation counting.

An exploratory metabolite identification was performed on selected plasma samples from HVs administered with a single dose of 18 mg risdiplam (SAD study) to identify the major circulating drug-related material. The high-resolution MS data acquired from SAD plasma samples of a representative individual up to 216 hours postdose were reinterrogated to address this concern. Of the 21 selected metabolites that met defined relevance criteria, high-resolution MS peak areas of 16 metabolites could be extracted in the revisited SAD study raw data and were plotted up to 216 hours (see Fig. 4).

Supplemental Table 2 shows a comparison of the metabolite-to-parent AUC ratios for the most abundant metabolites in plasma (M1 and M26) observed in the hADME study based on $^{14}$C and $^{12}$C, respectively.

Both the risdiplam metabolite-to-parent AUC ratios over 48 hours for the hADME study and over 216 hours for the SAD study were considered similar. The exploratory metabolite identification data derived from the representative individual over 216 hours postdose in the SAD study increased the confidence that the metabolites identified at the truncated $AUC_{0\text{-}48}$ in the hADME study were representative of $AUC_{inf}$. Additionally, a number of unexplained peaks in the radiochromatogram due to the low analytical sensitivity of the radioprofiling method were assigned to several minor metabolites after reanalyzing plasma samples from the SAD study. The analysis of the raw mass-spectral data up to 216 hours did not indicate any persistent metabolite with a significantly longer half-life than unchanged risdiplam, which indicated that metabolites did not accumulate after repeated doses of risdiplam and resolved the question raised by the Health Authority. Reassessing previously acquired data therefore revealed extended longitudinal results. The opportunity to reanalyze existing postacquisition data was pivotal in potentially preventing a costly follow-up clinical trial, which could have delayed the drug approval process.

## Investigating the Combination of Cytochrome P450 and Flavin-Containing Monooxygenase Contributions to Risdiplam Metabolism and Implications for Victim DDIs

In vitro metabolite identification showed that risdiplam was metabolized via an *N*-oxidation and oxidation-mediated piperazine ring degradation. Since there was no evidence of hydrolysis and conjugation biotransformation reactions, attention was focused on the metabolism of risdiplam by cytochrome P450 (P450) and flavin-containing monooxygenase (FMO) enzymes. Incubation of 10 μM radiolabeled risdiplam by recombinantly expressed P450 and FMO enzymes showed risdiplam can be metabolized by FMO1, FMO3, and CYP1A1, 3A4, and 3A7. Multiple metabolites (including M1) were generated by each of these enzymes. When sensitive liquid chromatography with tandem MS methods became available for risdiplam metabolite detection, a further assessment of risdiplam and M1 metabolism was made.

Figure 5 shows the relative amounts of metabolites M1, M2, and M5, which were detected in high abundance and formed in incubations using a panel of P450 and FMO enzymes. FMO1, FMO3, and CYP1A1, 2J2, 3A4, and 3A5 were the most active enzymes. The circulating metabolite M1 was further metabolized by many P450 and FMO enzymes (CYP1A1, 2C8, 2C19, 2J2, and 3A4; FMO1; and FMO3). Among these enzymes, CYP2J2, CYP3A4, FMO1, and FMO3 were most active in M1 metabolism (unpublished data). Individual enzyme turnover data can be extrapolated to estimate the fraction metabolized ($f_m$) when suitable scaling factors are known. However, this was not the case for a number of enzymes active in risdiplam metabolism at the time of performing the studies. To calculate intersystem extrapolation factors or relative activity factors, drug turnover rates and turnover rates for enzyme-selective substrates for the individual enzyme preparations and pooled HLMs are required. These approaches have been validated for several P450s, but others may lack established enzyme-selective probe substrates or may not be well represented by the pooled HLMs test system. For instance, CYP1A1 is known to be expressed in extrahepatic tissues and present in liver microsomes from some donors but is essentially inactive in pooled HLMs (Lang et al., 2019). CYP2J2 is

TABLE 1

M1 coverage in nonclinical pivotal toxicity studies at the respective NOAEL

| | Dose at NOAEL *mg/kg/day* | | M1 Exposure at NOAEL [$AUC_{0\text{-}24}$ in ng·h/ml] | | Animal vs. Human M1 Exposure Ratio* | |
|---|---|---|---|---|---|---|
| Species | M | F | M | F | M | F |
| Monkeys | 1.5 | 1.5 | 285 | 314 | 0.43 | 0.47 |
| Adult rats | 1 | 3 | 796 | 3195[†] | 1.19 | 4.78 |
| Rats (PND31) | 1.5 | 1.5 | 439 | 406 | 0.66 | 0.61 |
| RasH2 mice | 9 | 9 | 1690 | 1580 | 2.53 | 2.37 |
| Rabbits | NA | 4 | NA | 303 | NA | 0.45 |

*The M1 $AUC_{0\text{-}24,ss}$ at the mean exposure guidance in patients with SMA (2000 ng·h/ml; parent $AUC_{0\text{-}24,ss}$) was extrapolated by multiplying the parent $AUC_{0\text{-}24,ss}$ with the median M1/parent ratio (0.334) in patients with SMA at pivotal doses (i.e., M1 $AUC_{0\text{-}24,ss}$ = 2000 ng·h/ml × 0.334 = 668 ng·h/ml). The animal vs. human M1 exposure ratio is the ratio of the animal M1 $AUC_{0\text{-}24,ss}$ on the last day of dosing at the NOAEL dose divided by the extrapolated M1 $AUC_{0\text{-}24,ss}$ at the mean exposure guidance in patients with SMA (668 ng·h/ml).

[†]Plasma samples taken before incorporation of M1-preservation measures into bioanalytical methods. The M1 exposure was estimated from a corresponding PK bridging study as follows: M1 $AUC_{0\text{-}24}$ = (parent $AUC_{0\text{-}24}$ on the last day of dosing at the NOAEL dose) × (M1/parent ratio from PK bridging study).

AUC0-24, AUC from time 0 to 24 h; AUC0-24,ss, steady-state AUC from time 0 to 24 h; F, females; M, males; NA, not applicable; NOAEL, no observed adverse effects level; PK, pharmacokinetics; PND, postnatal daySMA, spinal muscular atrophy.

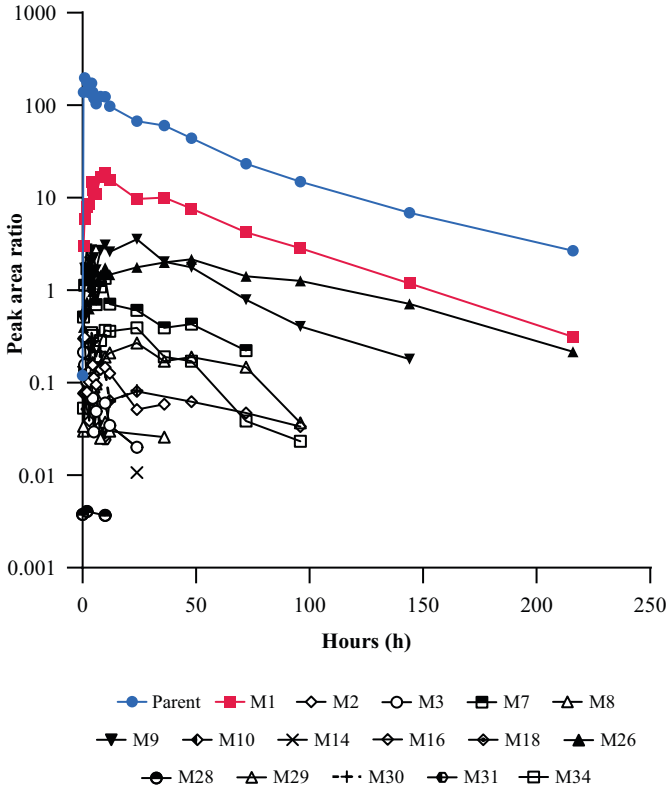


**Fig. 4.** Postacquisition, exploratory metabolite identification analysis in plasma levels of risdiplam and metabolites after a single oral dose of 18 mg risdiplam in one healthy volunteer.

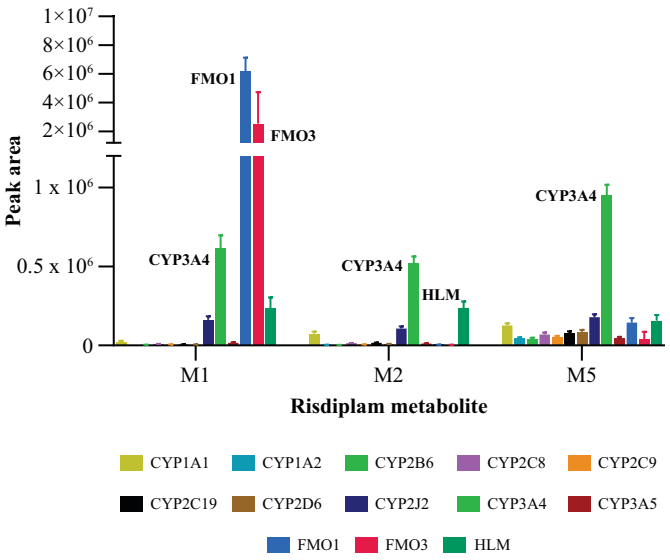


**Fig. 5.** Generation of specific metabolites on incubation of 1 μM risdiplam with individual P450 and FMO enzymes and HLMs. HLM, human liver microsome; FMO, flavin-containing monooxygenase; P450, cytochrome P450.

expressed in several extrahepatic tissues, including the heart, and has an important role to play in the regulation of arachidonic acid derivatives (Solanki et al., 2018). Recent studies have reported the discovery of selective CYP2J2 substrates (Zhao et al., 2021) and inhibitors (Phuc et al., 2017). The emerging characterization tools, tissue concentration measurements, and drug examples may enable a more quantitative estimation of the contributions of less-studied enzymes to drug metabolism in future.

Risdiplam was metabolized by human liver, kidney, and intestinal microsomes with 24%, 9%, and 2% turnover observed, respectively, after 1 hour of incubation (at a higher microsomal protein concentration of 1 mg/ml) (Supplemental Table 3). Under these experimental conditions, midazolam was turned over by >97%, <20%, and >97% by liver, kidney, and intestinal microsomes, respectively. These results indicated a differential enzymology of risdiplam with this CYP3A marker drug. The high relative rates of the hydroxylamine metabolite M1 formation and those of other metabolites formed by the kidney microsomes highlighted the possible involvement of FMO1 in the metabolism of risdiplam. Methimazole, an inhibitor of FMO enzymes (Störmer et al., 2000), reduced kidney microsomal metabolism by >90%. The data suggested that risdiplam was mainly metabolized by FMO1 in the kidney with only minor contributions from other enzymes. However, after accounting for the organ weight and blood flow, the scaled whole organ clearance of risdiplam in the kidney was ≤3% of hepatic clearance. This indicated that the actual contribution of FMO1 enzyme to risdiplam clearance was low even though the in vitro turnover by FMO1 was high, which showed the importance of translating the raw enzyme activities into likely human relevance.

In vitro studies were also performed to investigate the impact of inhibiting CYP3A and FMO enzymes on liver microsomal metabolism. Methimazole reduced human liver microsomal turnover by ∼75%, which is consistent with an important role for FMO3 in liver metabolism. As additional analytical methodologies became available, it was possible to examine the effect of inhibitors on the formation of the most abundant in vitro risdiplam primary metabolites M1, M2, and M5 at a more physiologically relevant concentration (1 μM; Supplemental Table 4). CYP3A inhibition by ketoconazole reduced the formation of these metabolites by 23%–62%, whereas methimazole inhibited their formation by 17%–46%, dependent upon the metabolite. This demonstrated that FMO and CYP3A enzymes are important contributors to risdiplam metabolism and provided potential $f_m$ ranges for planning a definitive in vivo DDI study. Since the time of performing these studies, the first demonstrations of chemical inhibitor effectiveness and application to $f_m$ estimation using long-term hepatocyte cultures have started to emerge (Chan et al., 2020). These approaches will give additional opportunities for $f_m$ estimation based on total drug depletion when such validation is available for a panel of selective inhibitors.

FMOs are important for the metabolic clearance of benzydamine, itopride, pargyline, ranitidine, olopatadine, xanomeline, albendazole, cimetidine, and ethionamide and are minor contributors to the metabolism of many other compounds (Krueger and Williams, 2005; Phillips and Shephard, 2020). However, there are few examples of clinical DDIs, and currently, no probe inhibitors for use in clinical DDI studies have been recommended (US Food and Drug Administration, 2020b). In a survey of enzymes involved in the metabolism of the FDA new drug applications between 2013 and 2016, FMO enzymes were listed as contributing to the metabolism of only 3 out of 98 cases (in which data were available), and investigation with clinical DDI studies was not reported for any of these (Yu et al., 2018). FMOs are generally viewed favorably as contributing enzymes to the metabolism of drugs, which was recently reiterated in the case study for ABT-126, which is mainly metabolized by FMOs (Liu et al., 2018). FMO induction is not well known, and few drugs that inhibit FMOs have been identified, which reduces the likelihood of DDIs (Cashman and Zhang, 2006). These positive aspects are also reflected in the smaller body of in vitro and clinical data available for FMOs compared with P450s. At the same time, the paucity of literature examples of FMO metabolism impacted

preclinical confidence in the accurate extrapolation of risdiplam in vitro data.

Although FMO3 activity can be assessed using benzydamine *N*-oxidation as a probe reaction (Lang and Rettie, 2000; Störmer et al., 2000), the scaling of FMO contributions to overall metabolism has not been well established to date. Obstacles here include a lack of clinical comparator data and uncertainties about the percentage of FMO3 enzyme activity remaining in HLM preparations due to thermal lability. With additional case reports of in vitro $f_m$ prediction and in vivo $f_m$ confirmation, confidence will be built in the estimation of FMO contributions to metabolism. A step in this direction was provided by Jones et al. (2017), who reported on the scaling of intrinsic clearance data for FMO-cleared drugs. Using HLM and HH intrinsic clearance data, they showed human clearance could be reasonably predicted, which was consistent with our experience with risdiplam. Risdiplam is therefore an important addition to the list of drugs with clinically important contributions from FMO enzymes and demonstrates that clearance scaling for an FMO/P450 substrate could be made effectively. This should help in the build-up of validation datasets needed for intrinsic clearance and $f_m$ predictions for FMO substrate drugs to become better accepted.

## Translating In Vitro–In Vivo–In Silico Data to First in-Human Trials

A PBPK model was used to calculate appropriate doses of risdiplam for the entry-into-human study. The safety and tolerability of these predicted doses were assessed in the SAD study (Sturm et al., 2019). PK data and DDI potential with risdiplam were also obtained to verify in vitro results and in silico predictions. Details regarding the PBPK model can be found in Table 2.

The PBPK model predicted almost complete absorption after oral administration of 0.6–18 mg risdiplam as oral solution (fraction absorbed $> 0.9$) and a volume of distribution at steady state of 4.1 l/kg in adult humans (Table 2). The predicted metabolic clearances in the kidney and intestine based on the turnover study were $\leq$3% of the predicted hepatic clearance and therefore were not included in the PBPK model. Consequently, the risdiplam clearance was modeled with the predicted plasma clearance of 7.3 l/h, which was based on hepatic metabolism scaled from the intrinsic clearance determined by the turnover in HepatoPac. This indicated low hepatic extraction (hepatic availability $> 0.9$) and negligible intestinal metabolism (intestinal availability $> 0.9$ based on CYP3A metabolism, and unbound fraction in enterocyte $= 1$). Overall, high bioavailability (approximately 0.9) was predicted for 0.6–18 mg of risdiplam administered as an oral solution. In the hADME study, approximately 14% and 17% of 18-mg orally administered [$^{14}$C]-risdiplam were recovered as unchanged risdiplam in the pooled feces collected over 168 and 840 hours, respectively (Fig. 2C), which is consistent with the predicted bioavailability.

In the SAD study in HVs, risdiplam was well tolerated up to the highest dose tested (18 mg), and the PK properties were linear over the entire dose range (Sturm et al., 2019). The predicted plasma clearance of 7.3 l/h was found to be in good agreement with the apparent clearance of 5.68 l/h estimated by a population PK model developed on the SAD study data (Supplemental Fig. 5; Supplemental Table 5) given the predicted high oral bioavailability of risdiplam. The total hepatic clearance was adjusted to the population PK model estimates and included a renal clearance of 0.33 l/h, which corresponded to approximately 5% of the total clearance.

Potential DDI by CYP3A inhibition was investigated by coadministration of risdiplam with itraconazole in HVs (Sturm et al., 2019). Based on these data, the PBPK model estimated a fraction of risdiplam metabolized by CYP3A of 20% (Sturm et al., 2019). The remainder of the metabolic clearance was assigned to hepatic metabolism through FMO3 enzyme according to the in vitro enzymology study for risdiplam ($f_m$ by FMO3 = 75%). The plasma concentration-time profiles and PK parameters simulated by the PBPK model of risdiplam showed good agreement with the observations in all doses investigated in the SAD study (Sturm et al., 2019) as shown in Fig. 6 and Table 3, respectively. Subsequently, the PBPK model was extrapolated to adult and pediatric patients with SMA (Cleary et al., 2021c) to support dose selection for therapeutic studies and DDI risk assessments (Cleary et al., 2021a).

## DDIs Risk Profile—Clinical Relevance of CYP3A Time-Dependent Inhibition and Emerging Transporters

DDIs occur when drugs taken in combination with other drugs cause unexpected side effects or efficacy because of modified drug exposure; their detection is therefore essential for patients on concomitant medications. These effects happen when DMEs, such as P450 enzymes or drug transporters, are inhibited or induced, which affects the

TABLE 2

Input parameters of risdiplam PBPK model

| Parameter | Value | Sources |
|---|---|---|
| Molecular weight | 401.5 g/mol | |
| Compound type | Diprotic base<br>pKa1 = 4.52<br>pKa2 = 6.82 | Measured |
| LogD* | 2.51 (pH = 7.4) | Measured |
| Permeability ($P_{eff}$) | 20.4 $\times 10^{-6}$ cm/s | Measured |
| B:P ratio | 1.3 | Measured |
| Protein binding | 89% | Measured |
| Absorption | | |
| $F_A$ | >0.9 | Predicted by ADAM model |
| $f_{u,gut}$ | 1 | (Yang et al., 2007) |
| Distribution | 4.1 l/kg | Full PBPK model with predicted Kp values (Rodgers and Rowland, 2006) |
| Metabolism | | |
| $CL_{int,CYP3A4}$ (µl/min/pmol) | 0.018 | According to itraconazole DDI study results (Sturm et al., 2019) |
| $CL_{int,FMO3}$ (µl/min/pmol) | 0.364 | Calculated based on in vitro and clinical study results |
| Elimination | | |
| $CL_R$ (l/h) | 0.33 | According to the observations in healthy individuals (Sturm et al., 2019) |

*The corresponding LogP is 2.61.

ADAM, advanced dissolution, absorption, and metabolism; B:P, blood to plasma; CLint, intrinsic clearance; CLR, renal clearance; DDI, drug-drug interaction; FA, fraction absorbed; fu,gut, unbound fraction in enterocyte; Kp, tissue-plasma partition coefficient; PBPK, physiologically based pharmacokinetic; Peff, effective permeability.

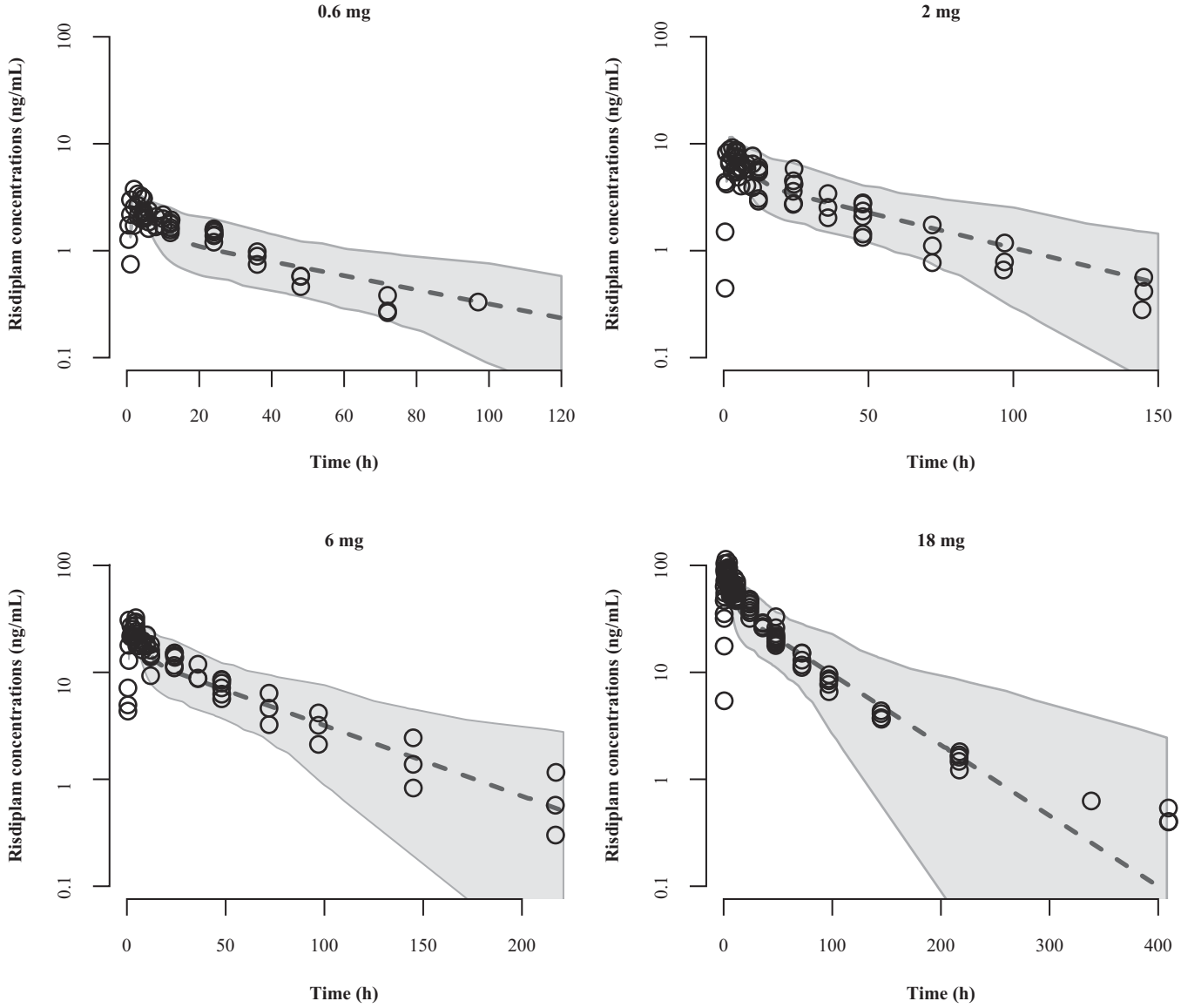


**Fig. 6.** Simulated and observed plasma concentrations of risdiplam after 0.6, 2, 6, or 18 mg as a single dose. The observations (open circles), 5th–95th percentiles (gray shades), and geometric means (gray dotted lines) of the simulated concentrations are shown.

pharmacokinetics of the administered drug. This can be conceptualized as "victim" drugs (whose pharmacokinetics are directly affected) or "perpetrator" drugs (which inhibit or induce enzymes/transporters and affect the pharmacokinetics of the victim). The case of terfenadine is one example of the victim-perpetrator DDI effect. Terfenadine was withdrawn from the market because of its elevated concentrations in plasma that resulted in life-threatening and fatal cardiac arrhythmia in some patients who were comedicated with ketoconazole (Honig et al., 1993). However, in some cases, perpetrator drugs have been coadministered as an intentional strategy to prolong victim drug plasma concentrations. Such is the case for human immunodeficiency virus–protease inhibitors, which are primarily metabolized by CYP3A. For example, when coadministered with ritonavir (strong CYP3A inhibitor), plasma exposures of protease inhibitors are boosted. It is now recommended as part of first-line treatment that low-dose ritonavir is codosed with human immunodeficiency virus–protease inhibitors (Hull and Montaner, 2011).

Regulatory bodies require a thorough evaluation of any possible drug interactions against both DMEs and membrane transporters prior to market approval (US Food and Drug Administration, 2018; Ishiguro et al., 2020). It has been recommended to use in vitro systems to investigate any potential DDIs. In silico studies (e.g., PBPK models) can be used and are accepted in lieu of some prospective DDI studies to predict moderate or weak perpetrator drugs on the exposure of the parent drug (US Food and Drug Administration, 2020a). As the major metabolite of risdiplam M1 was found to be MIST-relevant, risdiplam and M1 were both examined for P450 induction in HHs as well as for reversible (direct) and irreversible [time-dependent inhibition (TDI)] inhibition in HLMs. There was no significant induction of CYP1A2, 2B6, 2C8, 2C9, 2C19, and 3A4 at the mRNA level after incubation of risdiplam and M1 in primary HHs. Risdiplam and M1 also did not show direct inhibition of major P450 enzymes (1A2, 2B6, 2C8, 2C9, 2C19, and 2D6) except for CYP3A at concentrations of up to 12.5 and 10 μM, respectively. These concentrations are much higher than the maximum plasma concentration ($C_{max}$) values [184 ng/ml (0.46 μM)] after oral administration at the therapeutic dose of risdiplam, which indicates no clinically relevant direct inhibition on P450 substrates.

In vitro TDI parameters of risdiplam and M1 on CYP3A were measured. For risdiplam, the inhibitory constant ($K_I$) = 13 μM and in vitro inactivation rate constant = 0.065 minute$^{-1}$ whereas for M1, the $K_I$ =

TABLE 3

Comparison of predicted and observed PK parameters of risdiplam

| Dose | $C_{max}$ *ng/ml* | $t_{max}$ *h* | $AUC_{inf}$ *ng • h/ml* |
|---|---|---|---|
| 0.6 mg | | | |
| Observation | 2.82 | 3.0 | 86.7 |
| Prediction | 2.86 | 2.45 | 112 |
| 2 mg | | | |
| Observation | 8.33 | 3.0 | 294 |
| Prediction | 9.53 | 2.45 | 373 |
| 6 mg fasted | | | |
| Observation | 24.5 | 2.0 | 1080 |
| Prediction | 28.6 | 2.45 | 1120 |
| 18 mg | | | |
| Observation | 93.2 | 2.0 | 3290 |
| Prediction | 85.8 | 2.45 | 3360 |

Data are presented as geometric means except for $t_{max}$ (median).
AUCinf, AUC extrapolated to infinity; tmax, time to reach the maximum concentration $AUC_0$.inf, area under the plasma concentration−time curve extrapolated to infinity; tmax, time to reach the maximum concentration.

13.7 μM and inactivation rate constant = 0.063 $minute^{-1}$; Supplemental Table 6. However, there is some uncertainty over these values because the TDI effect did not reach saturation at the concentrations of risdiplam tested because of solubility limitations. Indeed, the estimated $K_I$ was higher than the maximal test substance concentration (12.5 μM) in the study, which indicated a level of uncertainty with the fitting performance. This could result in the overprediction of the TDI potency in the initial perpetrator DDI risk assessment. Moreover, in vitro TDI data measured from standard HLM assays frequently overpredict the magnitude of DDI (Eng et al., 2020) and fail to correctly categorize a drug as a weak, moderate, or strong inhibitor in vivo (Mao et al., 2012). A model system of HHs suspended in human plasma has been proposed to be an alternative in vitro system to more accurately assess CYP3A-mediated TDI-DDI risk. The HHs suspended in human plasma demonstrated a more reliable clinical DDI prediction for CYP3A TDI (Mao et al., 2012, 2016; US Food and Drug Administration, 2020a).

With a positive TDI result of risdiplam in HLMs, the PBPK model can be used to predict the magnitude of the DDI and investigate any DDI risk in future clinical studies. The model predicted an approximately 2-fold increase in AUC for midazolam (prototypical CYP3A substrate) in healthy adults, which was considered clinically relevant [FDA threshold; AUC ratio ≥ 1.25 (US Food and Drug Administration, 2020b)] and warranted further clinical investigations. However, results from the clinical DDI study in healthy adults showed that, in the presence of risdiplam, $C_{max}$ and AUC of midazolam were increased by 16% and 11%, respectively (Cleary et al., 2021b). The finding was not clinically relevant, and therefore dose adjustment for concomitantly used CYP3A substrates is not necessary.

In vitro–in vivo extrapolation methods to investigate membrane transporter interactions are mostly unavailable—with the exception of multidrug resistance mutation 1 (MDR1)—and therefore can present a challenge when studying and validating potential DDIs (Giacomini et al., 2010; Yoshida et al., 2017).

Risdiplam and M1 were screened in the relevant drug transporter assay as substrates. Both compounds were determined to be highly permeable molecules (>300 nm/s in LLC-PK1 or MCKII cells). Risdiplam was not a substrate of human MDR1 and was a weak substrate of human breast cancer resistance protein [BCRP; efflux ratio (ER) = 3.1] (Ratni et al., 2018). M1 was a weak-to-good substrate of human MDR1 (ER = 5.5) and a weak substrate of human BCRP (ER = 4.1). The in vitro hepatic uptake of risdiplam in HHs was not sensitive to an organic anion–transporting polypeptide inhibitor (Rifamycin SV, 100 μM) and, therefore, risdiplam was not considered an organic anion–transporting polypeptide substrate. The hepatic uptake is likely to be driven predominantly by passive diffusion, which is consistent with its high passive permeability. Overall, risdiplam and M1 did not present a clinically significant DDI risk related to drug-transport proteins as victims.

When risdiplam and M1 were screened against a panel of relevant transporter proteins as perpetrators, the results showed that risdiplam inhibited organic cation transporter 2 (OCT2), multidrug and toxin extrusion protein (MATE) 1, and MATE2-K, whereas M1 inhibited BCRP and MATE1 (Table 4). To assess the clinical relevance of these in vitro inhibition risks, regulatory bodies recommend: 1) for intestinal efflux (BCRP): calculating the drug level in the gastrointestinal tract as the oral dose divided by 250 ml and 2) for hepatic efflux (BCRP) and renal uptake (OCT2, MATE1, and MATE2-K): calculating the ratio of unbound plasma $C_{max}$ to the in vitro $IC_{50}$ (inhibitor concentration [I]/$IC_{50}$) (European Medicines Agency, 2020; US Food and Drug Administration, 2020a). The transporter-related clinical DDI risk can be excluded if the ratio [I]/$IC_{50}$ is lower than 0.02.

TABLE 4

Human DDI risk assessment for transport-proteins inhibition by risdiplam or M1

| Compound / Protein | $IC_{50}$ μ*M** | Total $C_{max}$ in Patients with SMA *ng/ml** | [I] μ*M*† | [I]/$IC_{50}$ | Threshold‡ |
|---|---|---|---|---|---|
| Risdiplam / OCT2 | 8.7 | Median = 184 (0.2 mg/kg, <2 yr) | 0.049 | **0.006** | 0.02 |
| | | Max observed = 364 | 0.097 | **0.011** | |
| Risdiplam / MATE1 | 0.15 | Median = 184 (0.2 mg/kg, <2 yr) | 0.049 | **0.33** | |
| | | Max observed = 364 | 0.097 | **0.65** | |
| Risdiplam / MATE2-K | 0.09 | Median = 184 (0.2 mg/kg, <2 yr) | 0.049 | **0.54** | |
| | | Max observed = 364 | 0.097 | **1.08** | |
| M1 / MATE1 | 14.8 | Median = 61 (0.2 mg/kg, <2 yr) | 0.011 | **0.0007** | |
| | | Maximum = 122 | 0.022 | **0.0015** | |
| M1 / BCRP | 2.3 | Median = 61 (0.2 mg/kg, <2 yr) | 0.011 | **0.0047** | |
| | | Maximum = 122 | 0.022 | **0.0094** | |

Embolden text indicate values above the [I]/$IC_{50}$ threshold.
*Risdiplam and M1 plasma concentrations at steady state at pivotal doses [SUNFISH study (NCT02908685): 0.25 mg/kg (body weight < 20 kg) or 5 mg; FIREFISH study (NCT02913482): 0.2 mg/kg].
The assessment was based on the median and maximum observed $C_{max}$ values in the FIREFISH study; $C_{max}$ values were lower in older patients in the SUNFISH study. Median M1 percentage vs. parent of 33.4 = ∼30% was assumed for calculating M1 $C_{max}$ values.
†[I] is the unbound plasma concentration (assuming free fraction in human plasma 10.7% for risdiplam and 7.4% for M1).
‡Most conservative [I]/$IC_{50}$ threshold above which require further investigation of the DDI potential by conducting a clinical DDI study (European Medicines Agency, 2020; US Food and Drug Administration, 2020a).
BCRP, breast cancer resistance protein; *C*max, maximum plasma concentration; DDI, drug-drug interaction; MATE, multidrug and toxin extrusion protein; OCT2, organic cation transporter 2; SMA, spinal muscular atrophy.

The approach to assess clinical relevance of BCRP inhibition was not applicable to risdiplam because M1 is a circulating metabolite and not detected in the feces of humans. For renal uptake, the static model recommended by the regulatory bodies revealed a potential clinically relevant risk only for risdiplam inhibition of both MATE1 and MATE2 with a calculated ratio exceeding the recommended 0.02 threshold (Table 4). However, static models are known to overpredict clinical DDIs (Filppula et al., 2019). Rather, a PBPK model could be an alternative strategy to further evaluate the DDI risk. MATE proteins are often referred to as "emerging" transporters and clinical case examples are rare. To date, as MATE-related DDIs are rare, there is no validated PBPK model available to assess MATE-related DDIs, which further prevented any quantitative extrapolation (Yoshida et al., 2017). Currently, the most validated victim is metformin, and the methodology to extrapolate a possible DDI to other substrates remains to be validated because of a lack of clinical comparator data (US Food and Drug Administration, 2020b). Most of the existing clinical evidence concerning MATE-related DDIs pertains to the inhibition of metformin renal clearance by cimetidine, pyrimethamine, or dolutegravir (Chu et al., 2018). The highest metformin AUC ratio (2.68) has been observed with pyrimethamine. Since metformin elimination is dependent mostly on a renal secretion by an active transporter and pyrimethamine acts as a strong and selective MATE inhibitor, this concrete clinical case can be considered the worst-case example known thus far. Fexofenadine, dofetilide, cephalexin, and procainamide are among other rare victim drugs affected by MATE-mediated DDIs with clinical data (Hillgren et al., 2013). Since these drugs are not a part of the standard of care for patients with SMA, the risk of DDI due to MATE was deemed to be minimal.

Quantitative extrapolation and clinical significance of in vitro findings for emerging transporters remain a challenge. New biomarker-informed strategies, for example assessing early clinical samples for serum creatinine levels for MATEs, can serve as an additional filter to minimize false negative and false positive predictions and can enable quantitative DDI predictions (Mathialagan et al., 2020).

## Conclusion

Assessing small molecules with complex ADME properties is not always straightforward. However, new technology and advancements to existing methods are allowing scientists to overcome longstanding challenges. Moreover, when in vitro studies, PBPK modeling, and clinical investigations are successively combined, a cohesive picture of the overall PK profile of a drug can be determined. This was exemplified here in the development of risdiplam. Despite low turnover, in vitro clearance of risdiplam was determined using a long hepatocyte coculture system. The PBPK model, with a robust description of ADME process, helped to define the doses to be assessed in the SAD study. The SAD trial was instrumental in assessing the safety and tolerability of risdiplam but also in verifying metabolic clearance, renal secretion, and potential DDI risks. The in vivo metabolic profiling of plasma samples from the SAD study, which were supplemented by in vitro data, appropriately informed the MIST-relevance of metabolites. This prevented potential delays in the program (e.g., bioanalytical method development, synthesis of standards, etc.) because these could be identified early in development. The SAD trial data were also crucial several years after its first analysis for investigating metabolites in plasma for up to 216 hours to ensure there were no persistent metabolites. Through this in vitro–in vivo–in silico strategy, the clinical development of risdiplam was accelerated, multiple PK questions were swiftly answered, and regulatory requirements for drug filing were fulfilled, all of which led to the FDA approval (US Food and Drug Administration, 2020c) and recent European Commission approval (European Medicines Agency, 2021) of risdiplam. We hope insights and perspectives can be gained from this case study to help investigators developing small-molecule drugs with challenging ADME profiles for the clinic.

## Acknowledgments

The authors would like to acknowledge Christoph Funk and Simone Schadt for their input throughout the risdiplam program. The authors would like to thank all the staff of the Spinal Muscular Atrophy Foundation and PTC Therapeutics for their collaboration, patients and families who have participated in the risdiplam program, staff of the clinical trial sites, staff around the world for their ongoing partnership and assistance, and Michelle B. Kim of MediTech Media for providing medical writing support, which was funded by F. Hoffmann-La Roche Basel AG, Switzerland, in accordance with Good Publication Practice (GPP3) guidelines (http://www.ismpp.org/gpp3).

## Authorship Contributions

*Participated in research design:* Poirier, Brink, Kletzl, Fowler, Mueller, Tuerck, Kratochwil.

*Conducted experiments:* Brink, Husser, Savage, Fowler, Heinig, Umehara, Ullah, Kratochwil.

*Performed data analysis:* Poirier, Brink, Husser, Savage, Cleary, Kletzl, Fowler, Günther, Umehara, Ullah, Mueller, Tuerck, Kratochwil.

*Wrote or contributed to the writing of the manuscript:* Fowler, Brink, Cleary, Poirier, Günther, Heinig, Husser, Kletzl, Kratochwil, Mueller, Savage, Stillhart, Tuerck, Ullah, Umehara.

## References

Cashman JR and Zhang J (2006) Human flavin-containing monooxygenases. *Annu Rev Pharmacol Toxicol* **46**:65–100.

Chan TS, Scaringella Y-S, Raymond K, and Taub ME (2020) Evaluation of erythromycin as a tool to assess CYP3A contribution of low clearance compounds in a long-term hepatocyte culture. *Drug Metab Dispos* **48**:690–697.

Chu X, Liao M, Shen H, Yoshida K, Zur AA, Arya V, Galetin A, Giacomini KM, Hanna I, Kusuhara H, et al.; International Transporter Consortium (2018) Clinical probes and endogenous biomarkers as substrates for transporter drug-drug interaction evaluation: perspectives from the International Transporter Consortium. *Clin Pharmacol Ther* **104**:836–864.

Cleary Y, Gertz M, Grimsey P, Günther A, Heinig K, Ogungbenro K, Aarons L, Galetin A, and Kletzl H (2021a) Model-based drug-drug interaction extrapolation strategy from adults to children: risdiplam in pediatric patients with spinal muscular atrophy. *Clin Pharmacol Ther* 10.1002/cpt.2384.

Cleary Y, Gertz M, Grimsey P, Günther A, Heinig K, Ogungbenro K, Aarons L, Galetin A, and Kletzl H (2021b) Model-based investigation of CYP3A enzyme inactivation effect of risdiplam in infants, children and adults with spinal muscular atrophy (SMA). *Clin Pharmacol Ther* **109**:S5–S88.

Cleary Y, Gertz M, Morcos PN, Yu L, Youdim K, Phipps A, Fowler S, and Parrott N (2018) Model-based assessments of CYP-mediated drug-drug interaction risk of alectinib: physiologically based pharmacokinetic modeling supported clinical development. *Clin Pharmacol Ther* **104**:505–514.

Cleary Y, Kletzl H, Grimsey P, Frey N, Silber Baumann H, Stillhart C, Poirier A, Heinig K, Fowler S, Ogungbenro K, et al. (2021c) Population and physiologically-based pharmacokinetic modeling of risdiplam in infants, children and adults with spinal muscular atrophy (SMA). *Clin Pharmacol Ther* **109**:S5–S88.

Da-Silva F, Boulenc X, Vermet H, Compigne P, Gerbal-Chaloin S, Daujat-Chavanieu M, Klieber S, and Poulin P (2018) Improving prediction of metabolic clearance using quantitative extrapolation of results obtained from human hepatic micropatterned cocultures model and by considering the impact of albumin binding. *J Pharm Sci* **107**:1957–1972.

Docci L, Klammers F, Ekiciler A, Molitor B, Umehara K, Walter I, Krähenbühl S, Parrott N, and Fowler S (2020) In vitro to in vivo extrapolation of metabolic clearance for UGT substrates using short-term suspension and long-term co-cultured human hepatocytes. *AAPS J* **22**:131.

Docci L, Parrott N, Krähenbühl S, and Fowler S (2019) Application of new cellular and microphysiological systems to drug metabolism optimization and their positioning respective to in silico tools. *SLAS Discov* **24**:523–536.

Eng H, Tseng E, Cerny MA, Goosen TC, and Obach RS (2020) Cytochrome P450 3A time-dependent inhibition assays are too sensitive for identification of drugs causing clinically significant drug-drug interactions: a comparison of human liver microsomes and hepatocytes and definition of boundaries for inactivation rate constants. *Drug Metab Dispos* **49**:442–450.

European Medicines Agency(2020) Guideline on the investigation of drug interactions https://www.ema.europa.eu/en/documents/scientific-guideline/guideline-investigation-drug-interactions-revision-1_en.pdf. Accessed July 2021.

European Medicines Agency(2021) EVRYSDI: Summary of Product Characteristics https://www.ema.europa.eu/en/documents/product-information/evrysdi-epar-product-information_en.pdf. Accessed July 2021.

Filppula AM, Parvizi R, Mateus A, Baranczewski P, and Artursson P (2019) Improved predictions of time-dependent drug-drug interactions by determination of cytosolic drug concentrations. *Sci Rep* **9**:5850.

Food and Drug Administration(2016) Safety Testing of Drug Metabolite: Guidance for Industry https://www.fda.gov/media/72279/download. Accessed July 2021.
Food and Drug Administration(2018) Drug Development and Drug Interactions https://www.fda.gov/drugs/drug-interactions-labeling/drug-development-and-drug-interactions. Accessed July 2021.
Food and Drug Administration(2020a) Clinical Drug Interaction Studies — Cytochrome P450 Enzyme- and Transporter-Mediated Drug Interactions Guidance for Industry https://www.fda.gov/media/134581/download. Accessed July 2021.
Food and Drug Administration(2020b) Drug Development and Drug Interactions: Table of Substrates, Inhibitors and Inducers https://www.fda.gov/drugs/drug-interactions-labeling/drug-development-and-drug-interactions-table-substrates-inhibitors-and-inducers. Accessed July 2021.
Food and Drug Administration(2020c) FDA approves oral treatment for spinal muscular atrophy https://www.fda.gov/news-events/press-announcements/fda-approves-oral-treatment-spinal-muscular-atrophy. Accessed July 2021.
Fowler S, Morcos PN, Cleary Y, Martin-Facklam M, Parrott N, Gertz M, and Yu L (2017) Progress in prediction and interpretation of clinically relevant metabolic drug-drug interactions: a minireview illustrating recent developments and current opportunities. *Curr Pharmacol Rep* **3**:36–49.
Giacomini KM, Huang S-M, Tweedie DJ, Benet LZ, Brouwer KLR, Chu X, Dahlin A, Evers R, Fischer V, Hillgren KM, et al.; International Transporter Consortium (2010) Membrane transporters in drug development. *Nat Rev Drug Discov* **9**:215–236.
Hillgren KM, Keppler D, Zur AA, Giacomini KM, Stieger B, Cass CE, and Zhang L; International Transporter Consortium (2013) Emerging transporters of clinical importance: an update from the International Transporter Consortium. *Clin Pharmacol Ther* **94**:52–63.
Holmberg AA, Ekdahl A, and Weidolf L (2014) Systemic exposure to the metabolites of lesogaberan in humans and animals: a case study of metabolites in safety testing. *Drug Metab Dispos* **42**:1016–1021.
Honig PK, Wortham DC, Zamani K, Conner DP, Mullin JC, and Cantilena LR (1993) Terfenadine-ketoconazole interaction. Pharmacokinetic and electrocardiographic consequences. *JAMA* **269**:1513–1518.
Hull MW and Montaner JS (2011) Ritonavir-boosted protease inhibitors in HIV therapy. *Ann Med* **43**:375–388.
Hutzler JM, Ring BJ, and Anderson SR (2015) Low-turnover drug molecules: a current challenge for drug metabolism scientists. *Drug Metab Dispos* **43**:1917–1928.
Ishiguro A, Sato R, and Nagai N (2020) Development of a new Japanese guideline on drug interaction for drug development and appropriate provision of information. *Drug Metab Pharmacokinet* **35**:12–17.
Jones BC, Srivastava A, Colclough N, Wilson J, Reddy VP, Amberntsson S, and Li D (2017) An investigation into the prediction of in vivo clearance for a range of flavin-containing monooxygenase substrates. *Drug Metab Dispos* **45**:1060–1067.
Jones H and Rowland-Yeo K (2013) Basic concepts in physiologically based pharmacokinetic modeling in drug discovery and development. *CPT Pharmacometrics Syst Pharmacol* **2**:e63.
Khetani SR and Bhatia SN (2008) Microscale culture of human liver cells for drug development. *Nat Biotechnol* **26**:120–126.
Kratochwil NA, Meille C, Fowler S, Klammers F, Ekiciler A, Molitor B, Simon S, Walter I, McGinnis C, Walther J, et al. (2017) Metabolic profiling of human long-term liver models and hepatic clearance predictions from in vitro data using nonlinear mixed-effects modeling. *AAPS J* **19**:534–550.
Krueger SK and Williams DE (2005) Mammalian flavin-containing monooxygenases: structure/function, genetic polymorphisms and role in drug metabolism. *Pharmacol Ther* **106**:357–387.
Lang D, Radtke M, and Bairlein M (2019) Highly variable expression of CYP1A1 in human liver and impact on pharmacokinetics of riociguat and granisetron in humans. *Chem Res Toxicol* **32**:1115–1122.
Lang DH and Rettie AE (2000) In vitro evaluation of potential in vivo probes for human flavin-containing monooxygenase (FMO): metabolism of benzydamine and caffeine by FMO and P450 isoforms. *Br J Clin Pharmacol* **50**:311–314.
Liu H, Stresser DM, Michmerhuizen MJ, Li X, Othman AA, Reed AD, Schrimpf MR, Sydor J, and Lee AJ (2018) Metabolism and disposition of a novel selective α7 neuronal acetylcholine receptor agonist ABT-126 in humans: characterization of the major roles for flavin-containing monooxygenases and UDP-Glucuronosyl Transferase 1A4 and 2B10 in catalysis. *Drug Metab Dispos* **46**:429–439.
Lorson CL, Hahnen E, Androphy EJ, and Wirth B (1999) A single nucleotide in the SMN gene regulates splicing and is responsible for spinal muscular atrophy. *Proc Natl Acad Sci USA* **96**:6307–6311.
Mao J, Mohutsky MA, Harrelson JP, Wrighton SA, and Hall SD (2012) Predictions of cytochrome P450-mediated drug-drug interactions using cryopreserved human hepatocytes: comparison of plasma and protein-free media incubation conditions. *Drug Metab Dispos* **40**:706–716.
Mao J, Tay S, Khojasteh CS, Chen Y, Hop CE, and Kenny JR (2016) Evaluation of time dependent inhibition assays for marketed oncology drugs: comparison of human hepatocytes and liver microsomes in the presence and absence of human plasma. *Pharm Res* **33**:1204–1219.
Mathialagan S, Feng B, Rodrigues AD, and Varma MVS (2020) Drug-drug interactions involving renal OCT2/MATE transporters: clinical risk assessment may require endogenous biomarker-informed approach. *Clin Pharmacol Ther* 10.1002/cpt.2089.
Mercuri E, Pera MC, Scoto M, Finkel R, and Muntoni F (2020) Spinal muscular atrophy - insights and challenges in the treatment era. *Nat Rev Neurol* **16**:706–715.
Phillips IR and Shephard EA (2020) Flavin-containing monooxygenase 3 (FMO3): genetic variants and their consequences for drug metabolism and disease. *Xenobiotica* **50**:19–33.
Phuc NM, Wu Z, O Y, Lee JH, Oh S, Song GY, and Liu KH (2017) LKY-047: first selective inhibitor of cytochrome P450 2J2. *Drug Metab Dispos* **45**:765–769.
Ratni H, Ebeling M, Baird J, Bendels S, Bylund J, Chen KS, Denk N, Feng Z, Green L, Guerard M, et al. (2018) Discovery of risdiplam, a selective survival of motor neuron-2 *(SMN2)* gene splicing modifier for the treatment of spinal muscular atrophy (SMA). *J Med Chem* **61**:6501–6517.
Rodgers T and Rowland M (2006) Physiologically based pharmacokinetic modelling 2: predicting the tissue distribution of acids, very weak bases, neutrals and zwitterions. *J Pharm Sci* **95**:1238–1257.
Schadt S, Bister B, Chowdhury SK, Funk C, Hop CECA, Humphreys WG, Igarashi F, James AD, Kagan M, Khojasteh SC, et al. (2018) A decade in the MIST: learnings from investigations of drug metabolites in drug development under the "Metabolites in Safety Testing" regulatory guidance. *Drug Metab Dispos* **46**:865–878.
Solanki M, Pointon A, Jones B, and Herbert K (2018) Cytochrome P450 2J2: potential role in drug metabolism and cardiotoxicity. *Drug Metab Dispos* **46**:1053–1065.
Störmer E, Roots I, and Brockmöller J (2000) Benzydamine N-oxidation as an index reaction reflecting FMO activity in human liver microsomes and impact of FMO3 polymorphisms on enzyme activity. *Br J Clin Pharmacol* **50**:553–561.
Sturm S, Günther A, Jaber B, Jordan P, Al Kotbi N, Parkar N, Cleary Y, Frances N, Bergauer T, Heinig K, et al. (2019) A phase 1 healthy male volunteer single escalating dose study of the pharmacokinetics and pharmacodynamics of risdiplam (RG7916, RO7034067), a SMN2 splicing modifier. *Br J Clin Pharmacol* **85**:181–193.
Umehara K, Cantrill C, Wittwer MB, Di Lenarda E, Klammers F, Ekiciler A, Parrott N, Fowler S, and Ullah M (2020) Application of the extended clearance classification system (ECCS) in drug discovery and development: selection of appropriate in vitro tools and clearance prediction. *Drug Metab Dispos* **48**:849–860.
Underhill GH and Khetani SR (2018) Advances in engineered human liver platforms for drug metabolism studies. *Drug Metab Dispos* **46**:1626–1637.
Yang J, Jamei M, Yeo KR, Tucker GT, and Rostami-Hodjegan A (2007) Prediction of intestinal first-pass drug metabolism. *Curr Drug Metab* **8**:676–684.
Yeo CJJ and Darras BT (2020) Overturning the paradigm of spinal muscular atrophy as just a motor neuron disease. *Pediatr Neurol* **109**:12–19.
Yoshida K, Zhao P, Zhang L, Abernethy DR, Rekić D, Reynolds KS, Galetin A, and Huang SM (2017) In vitro-in vivo extrapolation of metabolism- and transporter-mediated drug-drug interactions-overview of basic prediction methods. *J Pharm Sci* **106**:2209–2213.
Yu J, Zhou Z, Tay-Sontheimer J, Levy RH, and Ragueneau-Majlessi I (2018) Risk of clinically relevant pharmacokinetic-based drug-drug interactions with drugs approved by the U.S. Food and Drug Administration between 2013 and 2016. *Drug Metab Dispos* **46**:835–845.
Zhang X, Yang Y, Grimstein M, Fan J, Grillo JA, Huang SM, Zhu H, and Wang Y (2020) Application of PBPK modeling and simulation for regulatory decision making and its impact on US prescribing information: an update on the 2018-2019 submissions to the US FDA's Office of Clinical Pharmacology. *J Clin Pharmacol* **60** (Suppl 1):S160–S178.
Zhao T, Chen Y, Wang D, Wang L, Dong P, Zhao S, Wang C, Meng Q, Sun H, Liu K, et al. (2021) Identifying the dominant contribution of human cytochrome P450 2J2 to the metabolism of rivaroxaban, an oral anticoagulant. *Cardiovasc Drugs Ther* 10.1007/s10557-020-07129-z.

**Address correspondence to:** Agnès Poirier, Pharmaceutical Sciences, Roche Pharma Research and Early Development, Roche Innovation Center Basel, F. Hoffmann-La Roche Ltd, Grenzacherstrasse 124, 4070 Basel, Switzerland. E-mail: Agnes.poirier@roche.com

# Supplemental Materials

## Addressing today's ADME challenges in the translation of in vitro absorption, distribution, metabolism and excretion characteristics to human: A case study of the *SMN2* mRNA splicing modifier risdiplam

Stephen Fowler*, Andreas Brink*, Yumi Cleary, Andreas Günther, Katja Heinig, Christophe Husser, Heidemarie Kletzl, Nicole Kratochwil, Lutz Mueller, Mark Savage, Cordula Stillhart, Dietrich Tuerck, Mohammed Ullah, Kenichi Umehara, Agnès Poirier

*These authors contributed equally to this work.

# Table of Contents

# Methods

## Metabolic clearance prediction for risdiplam, a low-clearance compound

### Metabolic stability

A suspension of human liver microsomes (HLMs) (0.636 mg protein/mL) was incubated with risdiplam (10 µM) for up to 1 h. From the suspension, aliquots were removed at time 0, 30 mins and 1 h and the reaction was quenched with ice-cold acetonitrile (1:1). Similarly, a suspension of hepatocytes ($0.5x10^6$ viable cells/mL) was incubated with risdiplam (10 µM) for up to 3 h. Aliquots were removed at time 0, 30 mins, 1 h, and 3 h and quenched with ice-cold acetonitrile (1:1). Samples were centrifuged and the supernatant was analyzed using ultra-performance liquid chromatography (UPLC) combined with quadrupole time of flight mass spectrometry (Waters, Manchester, UK, LC-MS). Samples were injected onto a CSH C18 UPLC column (1.7 µm, 2.1 x 100 mm) at 40°C. Mobile phase A was a water:methanol mixture (95:5 v/v) with 0.1% formic acid and mobile phase B was 100% acetonitrile with 0.1% formic acid. Samples were eluted using the UPLC optimized conditions (described below) at a flow rate of 200 µL/min for a total run time of 20 mins.

| Time (mins) | %A | %B |
|---|---|---|
| 0 | 100 | 0 |
| 2 | 100 | 0 |
| 10 | 50 | 50 |
| 12 | 2 | 98 |
| 14 | 2 | 98 |
| 16 | 100 | 0 |
| 20 | 100 | 0 |

### Clearance determination

HepatoPac® cultures were obtained from BioIVT (Westbury, NY, USA) and the clearance determination was conducted as described previously (Ballard et al., 2020), (Kratochwil et al., 2017). HepatoPac® cultures containing 3200 (in a 96-well plate) hepatocytes per well (donor specification [3121A]) were allowed to recover for 2 days after shipment; medium was changed and cultures kept in 10% $CO_2$ atmosphere at 37°C. Albumin and urea production were assessed to ensure good hepatic functionality (32 $\mu g \cdot day^{-1}$ Mio cells-1 and 290 $\mu g \cdot day^{-1}$ Mio cells-1 at Day 8 of culture, respectively) as described by Khetani et al. (Khetani and Bhatia, 2008).

A total hepatocyte protein content of 0.05 $mg \cdot mL^{-1}$ (0.0032 mg per well) was applied for the 96-well format. Cultures were washed with 64 µL serum-free HepatoPac® Dulbecco's Modified Eagle's Medium prior to the addition of risdiplam at concentrations of 0.3 and 1 µM. Incubations containing only mouse fibroblast cells served as controls as they occupy 75% of the surface area of the HepatoPac® format (Khetani and Bhatia, 2008). Risdiplam depletion was assessed over 7 days of the culture.

Risdiplam was quantified using liquid chromatography with tandem mass spectrometry (LC-MS/MS). A high-performance liquid chromatography (HPLC) system consisting of Shimadzu 30AD pumps and an HTS CTC PAL autosampler was used. The HPLC was coupled to a Sciex 6500-QTrap mass spectrometer equipped with a TurboIonSpray source. IonSpray voltage was set at 5500V in positive mode and –4500V in negative mode. Samples were centrifugated and aliquots (5 µL) were injected onto a Supelco Ascentis Express C18 column (20 cm x 2 mm with 2.7 µm particle size) at 70°C. Mobile phase A was a water:methanol mixture (95:5 v/v) with 0.5% formic acid and mobile phase B was 100% methanol. Samples were eluted using a gradient from 0–95% mobile phase B in 0.74 mins at a flow rate of 550 µL/min for a total run time of 1.5 mins.

Data were analyzed using Analyst 1.6.2 software (AB Sciex Pte Ltd, Singapore). Intrinsic clearance determination and direct scaling of the predicted *in vivo* clearance in plasma of risdiplam were done as described elsewhere [Kratochwil et al. (2017)]. For risdiplam, a plasma protein binding value of 0.11 and a blood to plasma ratio of 1.3 were applied for the direct scaling approach, where one assumes that the fraction unbound in plasma is equal to the fraction unbound in the *in vitro* system.

## Low *in vitro* turnover of risdiplam warranted confirmation of metabolites in safety testing (MIST)-relevant metabolites in early human plasma samples

### Metabolite identification

***In vitro assays to assess metabolism of risdiplam in several species***

*In vitro* metabolism of risdiplam was studied using liver microsomes and hepatocytes from humans, rats, cynomolgus monkeys, mice and rabbits and using recombinant human P450 enzymes (1A2, 2A6, 2B6, 2C8, 2C9, 2C19, 2D6, 2E1, 3A4). Liver microsomes (0.636 mg protein/mL) were incubated for 0, 30, and 60 mins, P450s (150 nM) at 0, 10 and 30 mins, and hepatocytes ($0.5x10^6$ viable cells/mL, in suspension) at 0, 30, 60 and 180 min. *In vitro* incubates were analyzed by UPLC combined with quadrupole time of flight mass spectrometry with reference to the available authentic standards to enable a cross-species comparison of metabolism. For metabolite identification, additional experiments were performed using HPLC in combination with an Orbitrap mass spectrometer.

### Human absorption, distribution, metabolism, and excretion (hADME) study – Excretion balance and metabolite profiling in human plasma

An open-label, non-randomized study investigating the excretion balance, PK and metabolism of a single dose of 18 mg of [$^{14}$C]-labeled risdiplam with ~0.75 MBq (20 µCi)-labeled risdiplam in six healthy male individuals 35–65 years of age (inclusive) was carried out (NCT03036501). A dose of 18 mg risdiplam did not result in any safety concerns, including no appreciable changes in vital signs, electrocardiogram (ECG) or laboratory values in a previous single-ascending-dose study (SAD, NCT02633709). Individuals were admitted on Day 1 of the study and 18 mg of [$^{14}$C]-labeled risdiplam was orally administered as a drinking solution under fasted conditions. Standard meals were provided throughout. Individuals remained in the clinical unit for ≥336 h after study drug administration. Safety parameters were measured including incidence and severity of adverse events (AEs), incidence of laboratory abnormalities based on hematology, clinical chemistry and urinalysis, ECG, vital signs and ophthalmologic assessments.

Urine and feces were quantitatively collected at specified time intervals until the release criterion was met (≥90% of total administered radioactivity recovered in urine and feces, as determined by liquid scintillation quick counts). Individuals were discharged on Day 15 provided release criterion were met; if criteria were not met individuals remained until they were but no longer than a further 7 days (Day 22). If criteria were not met on Day 22, then excreta collection continued quantitatively at 24-h intervals at home. Excreta collection stopped once release criteria were met, or at the latest on Day 36.

Blood samples were collected at specified timepoints to calculate PK parameters of [$^{12}$C]-risdiplam. Plasma concentrations of [$^{12}$C]-risdiplam were measured using LC-MS/MS; [$^{14}$C]-risdiplam radioactivity was determined in blood, plasma, urine and feces by liquid scintillation chromatography.
Approval for this study was obtained from the Institutional Review Board/Ethics Committee and the study was conducted in accordance with the Declaration of Helsinki and Good Clinical Practice guidelines described in the protocol. All individuals provided informed consent and completed screening procedures.

### Metabolite identification at later time points and implications for regulatory approval of risdiplam

An exploratory metabolite identification was performed on selected plasma samples from healthy volunteers dosed with a single dose of 18 mg risdiplam in the SAD study (Sturm et al., 2018) in order to identify the major circulating drug-related material. For a representative individual subject up to 216 h post-dose, the SAD plasma samples were analyzed using high resolution mass spectrometry (HRMS) applying a generic acquisition mode that acquired untargeted high-resolution full scan MS raw data combined with data-dependent collision-induced dissociation. This high-resolution tandem MS approach records m/z of all detectable drug-related components eluting during chromatography, as well as of its fragment ions. Once captured, such data can be re-interrogated at any time by post-acquisition analyses, e.g. extracting metabolite traces when new information accumulates in additional studies (e.g. hADME). The archived HRMS raw data of risdiplam were reanalyzed in response to a health authority question by extracting peak area ratios of selected metabolites which met the following criteria:

– was observed in excreta pools in the hADME study amounting to >1% in feces or urine

– was observed in plasma by the radioprofiling method in the hADME study

– was observed as *in vitro* metabolite in any human hepatic preparation (microsomes, hepatocytes, CYP450 [CYP] enzymes).

## Investigating the combination of CYP and flavin-containing monooxygenase (FMO) contributions to risdiplam metabolism and implications for victim DDIs

### $^{14}$C-risdiplam metabolism by human liver, kidney and intestinal microsomes

| | |
|---|---|
| Test substrates | $^{14}$C-risdiplam (10 µM), midazolam (1 µM) |
| Test inhibitors | Ketoconazole (1 µM), methimazole (1 mM) |
| Incubation systems | • 1 mg/mL HLM (150 donor mixed gender pool HLM [Corning, Lot:38290]) tested in presence and absence of test inhibitors<br>• 1 mg/mL human kidney microsomes (mixed donor pool [BioIVT lot YCD])<br>• 1 mg/mL human intestinal microsomes (mixed donor pool [Corning lot 40883004])<br>• 100 mM potassium phosphate buffer, pH 7.4,<br>• NADPH (1 mM) |

In a reaction volume of 1 mL of 100 mM potassium phosphate buffer, 10 µM of $^{14}$C-risdiplam or control substrate was incubated with 1 mg/mL of human liver, intestine or kidney microsomes at pH 7.4. Solutions were prewarmed at 37°C for 10 mins before substrate addition ($t_0$). The reactions were initiated with NADPH (1 mM), mixed, then immediately after 300 µL aliquot was removed and quenched with 600 µL of quench reagent. A second aliquot (300 µL) was removed and quenched with 600 µL of quench reagent after 1 h. The samples were cooled on ice for 1 h, centrifuged for 10 mins at 20,000 g and the supernatant removed. The supernatant (100 µL) was then analyzed by HPLC with chromatogram fractionation and offline solid scintillation counting. Midazolam (1 µM) was used as the control compound. For midazolam samples, reactions were quenched with 2 volumes of acetonitrile containing internal standards and analyzed by LC-MS/MS.

### $^{14}$C-risdiplam metabolism by CYP and FMO enzymes

| | |
|---|---|
| Test substrates | • $^{14}$C-Risdiplam (10 µM)<br>• Midazolam (1µM)<br>• Tacrine (CYP1A1)<br>• Tacrine (CYP1A2)<br>• Bupropion (CYP2B6)<br>• Amodiaquine (CYP2C8)<br>• Diclofenac (CYP2C9)<br>• *S*-mephenytoin (CYP2C19)<br>• Dextromethorphan (CYP2D6)<br>• Midazolam (CYP3A4, CYP3A5 and CYP3A7)<br>• Benzydamine (FMOl and FM03)<br>All incubations used 1 µM of positive control substrate with the exceptions of bupropion (10 µM), *S*-mephenytoin (2 5µM). |
| Incubation systems | • 1 mg/mL HLM (150 donor mixed gender pool HLM [Corning, Lot:38290])<br>• 200 pmol/mL individual CYP enzymes or 0.25 mg/mL SF9 membranes expressing FMOs<br>• 100 mM potassium phosphate buffer, pH 7.4<br>• NADPH (1 mM) |

In a total reaction volume of 1 mL of buffer, the incubations systems (including NADPH) were prewarmed for 5 mins to 37°C before being initiated by the addition of $^{14}$C-risdiplam or test substrates. After 1 h of incubation, an aliquot (300 µL) was removed from each reaction mix and quenched with the addition of 600 µL of pure methanol. Samples were chilled on ice for 1 h before centrifugation (20,000 g, 10 mins). The supernatant was removed and 100 µL analyzed by radio-HPLC (risdiplam) with chromatogram fractionation into 'Luma' plates. Radioactivity of the sample was determined by solid scintillation counting. Positive control substrate metabolism was analyzed by LC/MS-MS.

### Unlabeled risdiplam metabolism by individual CYP and FMO enzymes

| | |
|---|---|
| Test substrates | • Risdiplam and M1 (1 µM)<br>• Tacrine (CYP1A1)<br>• Tacrine (CYP1A2)<br>• Bupropion (CYP2B6)<br>• Amodiaquine (CYP2C8)<br>• Diclofenac (CYP2C9)<br>• *S*-mephenytoin (CYP2C19)<br>• Dextromethorphan (CYP2D6)<br>• Astemizole (CYP2J2)<br>• Midazolam (CYP3A4 and CYP3A5)<br>• Benzydamine (FMOl and FMO3)<br>All incubations used 1 µM positive control substrate with the exceptions of bupropion (10 µM), *S*-mephenytoin (25 µM), astemizole (10 µM). |
| Incubation systems | • Recombinantly expressed individual enzymes sourced from Corning-Gentest at concentrations of 100 pmol/mL (with 0.5 mg/mL membrane protein for FMO enzymes) and 1 mg/mL HLM (150 donor mixed gender pool HLM [Corning, Lot:38290])<br>• 100 mM potassium phosphate buffer, pH 7.4<br>• NADPH (1 mM) |
| Incubation time | 15 mins |

Incubation systems were warmed to 37°C over 5 min. The reaction was initiated by the addition of the cofactor. For risdiplam and M1 incubations, an aliquot (40 µL) of each incubate was removed after 15 mins and

quenched with 300 µL acetonitrile containing deuterated risdiplam and deuterated risdiplam-M1 as internal standards. For positive control incubations, 125 µL aliquots were removed at 3 and 15 mins and quenched with 125 µL cold acetonitrile containing $D_6$-midazolam as an internal standard.

Quenched samples were cooled for 1 h and then centrifuged. The supernatant was removed and 1 µL of each sample was analyzed by LC-MS/MS using a Waters Vion IMS Q-Tof mass spectrometer for risdiplam samples and an AB Sciex API6500 triple quadrupole mass spectrometer for positive control substrates.

Drug substances and metabolites were analyzed. Metabolite peak area ratios vs internal standard were used in data analysis.

### Effect of CYP-selective chemical inhibitors on metabolism of unlabeled risdiplam by HLM

| | |
|---|---|
| Test substrates | • Risdiplam and risdiplam M1 (1 µM)<br>• Control cocktail 1: 1 µM tacrine, 10 µM bupropion, 1 µM dextromethorphan<br>• Control cocktail 2: 1 µM diclofenac, 1 µM midazolam, 1 µM amodiaquine<br>• Control cocktail 3: 25 µM *S*-mephenytoin |
| Test inhibitors | • 0.5 µM α-naphthoflavone<br>• 10 µM ticlopidine<br>• 3 µM montelukast<br>• 10 µM sulfaphenazole<br>• 2 µM benzylphenobarbital<br>• 1 µM quinidine<br>• 1 µM ketoconazole<br>• 1 mM methimazole |
| Incubation system | • HLM (150-donor mixed gender pool, 1 mg/mL final concentration, [Corning, Lot:38290])<br>• 100 mM potassium phosphate buffer, pH 7.4<br>• NADPH (1 mM) |

Incubation systems were warmed to 37°C over 5 mins. The incubations began with the addition of the cofactor. Risdiplam and M1 incubations: 40 µL aliquots of each incubation removed at 3 and 15 mins and added to 300 µL acetonitrile containing deuterated risdiplam and deuterated risdiplam-M1 as internal standards. Positive control incubations: 125 µL aliquots were removed at 3 and 15 mins and added to 125 µL cold acetonitrile containing $D_6$-midazolam as internal standard.

Quenched samples cooled for 1 h were then centrifuged, supernatant removed and 1 µL of each sample was analyzed by LC-MS/MS using a Waters Vion IMS Q-Tof mass spectrometer for risdiplam samples and an AB Sciex API6500 triple quadrupole mass spectrometer for positive control substrates.

Drug substances and metabolites were analyzed. Metabolite peak area ratios vs internal standard were used in data analysis. The effect of the inhibitory compounds on the metabolite formation was assessed.

## DDIs risk profile – clinical relevance of CYP3A time-dependent inhibition (TDI) and emerging transporters

### Direct inhibition of CYP enzymes

The CYP inhibition potential of risdiplam (up to 12.5 µM) and M1 (up to 10 µM) on the CYP enzymes 1A2, 2B6, 2C8, 2C9, 2C19, 2D6 and 3A4/5 was determined at HLM concentrations ranging from 0.02 to 0.3 mg/mL and for ≤10 mins incubation time at 37 °C, supplemented with 1 mM NADPH (n=2). The following marker substrates at the concentrations close to the historical Michaelis-Menten constant ($K_m$) values were used in HLM incubations: 40 µM phenacetin (CYP1A2, acetaminophen formation); 80 µM bupropion (CYP2B6, OH-bupropion formation); 1.5 µM amodiaquine (CYP2C8, *N*-desethylamodiaquine formation); 5 µM diclofenac (CYP2C9, 4'-OH diclofenac formation); 40 µM *S*-mephenytoin (CYP2C19, 4'-OH *S*-mephenytoin formation);

5 μM dextromethorphan (CYP2D6, dextorphan formation); 3 μM midazolam (CYP3A4/5, 1'-OH midazolam formation) and 50 μM testosterone (CYP3A4/5, 6β-OH testosterone formation). The $IC_{50}$ values were determined by non-linear regression using XLfit (IDBS; Surrey, United Kingdom) or Microsoft Excel according to the following equation:

$$\%\ remaining\ activity = Min + \frac{Max-Min}{1+\frac{IC50^{\gamma}}{x}} \quad (1)$$

where *Min* and *Max* represent the minimum and maximum values for % remaining enzyme activity (specific metabolite formation), respectively. $IC_{50}$ is the inhibitor concentration ($x$) associated with 50% of the enzyme activity inhibition. $\gamma$ shows the slope factor

## TDI of CYP enzymes

For the CYP3A4/5 mechanism-dependent inhibition assessment, risdiplam and M1 (0.1 to 12.5 or 10 μM) were pre-incubated at 37°C for 0, 4, 15, 30, 45 and 60 mins. After pre-incubation, the microsomal incubations were diluted 10-fold with buffer containing the probe substrates (15 μM midazolam) and 1 mM NADPH, and then incubated at 37°C for 5 mins. The respective HLM concentrations during pre-incubation were 0.2 mg/mL (n=2). The natural logarithm of the residual activity was plotted over the pre-incubation time for each test article concentration. The first order rate constant for inactivation ($k_{obs}$) was estimated from slopes of the linear portion of the curves. The maximal rate of enzyme inactivation ($k_{inact}$) and the test substance concentration resulting in 50% of the maximum enzyme inactivation ($K_I$) were determined using non-linear regression with GraphPad Prism software version 6.01 (GraphPad Software Inc., San Diego, CA) as follows:

$$kobs = \frac{KI\times[I\}}{kinact+[I]} \quad (2)$$

where [I] is the inhibitor (test substance) concentration. Of note, estimation of $K_I$ and $k_{inact}$ for CYP enzymes other than CYP3A4/5 was not performed. The respective $IC_{50}$ of the parent drug and M1 against the probe enzyme activities was not shifted to the lower value after the pre-incubation.

## Induction of CYP enzymes

The induction potential of risdiplam and M1 on CYP1A2, 2B6, 2C8, 2C9, 2C19 and 3A4 were evaluated using three individual liver donors. Cryopreserved primary liver cells (male and female; mixed) were reconstituted in a tube containing pre-warmed InVitroGRO cryopreserved plateable medium at 37°C (BioreclamationIVT) and seeded on a 96-well collagen coated plate at a seeding density of 0.35 x $10^6$ hepatocytes/mL. The plate was incubated at 37°C for 4 h before the seeding medium was replaced with supplemented Williams E medium without serum. The cells were cultured for a further 24 h before addition of the test compound in serum-free culture media (0.1 % DMSO content). Positive control inducers (100 μM omeprazole for CYP1A2, 1000 μM phenobarbital for CYP2B6 and 50 μM rifampicin for CYP2C8/2C9/2C19/3A4) were incubated alongside the test compounds. The experiment was performed in triplicate at 0.001–1 μM risdiplam and M1, or control compounds at the designated concentrations stated as above. Negative control wells were also included on each plate consisting of the vehicle alone (0.1 % DMSO). The cells were exposed to the solutions for 48 h. Upon completion of the dosing period, the hepatocytes were washed twice with the incubation media.

The hepatocytes were then lysed, and total RNA isolation was performed using the KingFisher Flex nucleic acid purification system (ThemoScientific, Waltham, MA). Quantitative polymerase chain reaction (PCR) analysis was performed on cDNA, using Applied Biosystems (Waltham, MA) designed TaqMan® gene expression assays for the target genes CYP1A2, 2B6, 2C8, 2C9, 2C19, 3A4 and endogenous control (18S ribosomal RNA). Following a reverse transcription (RT) assay, a PCR assay was conducted using a QuantStudio 5 Real Time PCR System (ThermoFisher, Carlsbad, CA).

Relative fold mRNA expression levels of the target genes were determined based on the threshold cycle (CT) data of target gene relative to endogenous control for each reaction (ΔCT), normalized to the negative control (ΔΔCT). Fold induction is calculated using the $2^{-\Delta\Delta Ct}$ method.

## Drug transport protein assays

*Uptake assays (hepatocytes & over-expressed cells)*

For hepatocyte uptake, three wells were used as one set (i.e. n=3 per treatment). The medium was removed from the wells by aspiration and the wells were washed once with 1 mL of Hank's balanced salt solution (HBSS, InVitrogen/GIBCO) at 37°C. The uptake experiment was started by aspiration of wash buffer and adding 300 µL of pre-warmed 37°C HBSS/HEPES pH 7.4 solution containing the test compound, with and without the addition of Rifamycin SV (100 µM). It was ensured that the medium (300 µL) covered the entire cell surface area and the plate was transferred to a 37°C heating block. After the set duration of incubation (1–30 mins) the transport was immediately stopped by addition of 1 mL ice-cold phosphate-buffered saline (PBS, containing 0.2% bovine serum albumin ([BSA]) to each well and the solution was removed by aspiration. The transport was stopped by lowering the temperature to 4°C and dilution, while BSA was included in the washing buffer to minimize background due to unspecific binding of radioactive compound to the surface of the cells. The wells were washed twice with 2 mL of 37°C PBS (0.2% BSA). Finally, the wells were washed with 37°C PBS (about 3 mL in total, to remove added BSA protein). Special care was taken not to disrupt the cell monolayer during the wash steps. For intracellular sampling, 0.3 mL of ACN/water (75/25) containing internal standard were added to solubilize the cells. After incubation for 15 mins at room temperature on a shaking block, the solubilized cell lysate was transferred to a MTP 96 Eppendorf Twintec V plate and was subsequently measured using LC/MS/MS. An average protein content was determined from an additional plate by lysing the cells with Triton 1% and using the Pierce BCA assay with BSA as standard.

The monolayer assays were performed using parental and transfected MDCKII cell monolayers. Uptake experiments were performed using HEK293FT cells stably expressing the human OATP1B1, OATP1B3 or OAT3 uptake transporters, CHO cells stably expressing the human OAT1 or OCT2 uptake transporters, MDCKII cells stably expressing the human MATE1 or MATE2-K transporters. Mock transfected HEK293FT cells, parental CHO cells and CAT-transfected MDCKII cells were used as respective negative controls. Cells were cultured at 37 ± 1°C in an atmosphere of 95:5 air: $CO_2$ and were plated onto standard 96-well tissue culture plates.

Before the experiment, the medium was removed, and the cells were washed twice with 100 µL of HK buffer at pH 7.4 (or pH 8.0 for MATE1 and MATE2-K). Uptake experiments were carried out at 37 ± 1°C in 50 µL of HK buffer (pH 7.4 or pH 8.0 for MATE1 and MATE2-K) containing the probe substrate and the TA or solvent. The organic solvent concentrations were equal in all wells and did not exceed 1% (v/v).

After the experiment, cells were washed twice with 100 µL of ice-cold HK buffer and lysed with 50 µL of 0.1 M NaOH. Radiolabeled probe substrate transport was determined by measuring an aliquot (35 µL) from each well for liquid scintillation counting.

**Table S1. Parameters of uptake transporter assays.**

| Transporter | Applying assay protocol | Incubation time (mins) | Probe substrate | Reference inhibitor |
|---|---|---|---|---|
| Human OATP1B1 | UPT-HEK293-OATP1B1-E217βG | 3 | E217βG (1 μM) | Rifampicin (50 μM) |
| Human OATP1B3 | UPT-HEK293-OATP1B3-CCK8 | 10 | CCK-8 (0.11 μM) | Rifampicin (50 μM) |
| Human OAT1 | UPT-CHO-OAT1-PAH | 3 | PAH (5 μM) | Benzbromarone (200 μM) |
| Human OAT3 | UPT-HEK293FT-OAT3-E3S | 1 | E3S (1 μM) | Probenecid (500 μM) |
| Human OCT2 | UPT-CHO-OCT2-Metf | 10 | Metformin (10 μM) | Verapamil (100 μM) |
| Human MATE1 | UPT-MDCKII-MATE1-metformin | 15 | Metformin (10 μM) | Pyrimethamine (1 μM) |
| Human MATE2-K | UPT-MDCKII-MATE2K-metformin | 15 | Metformin (10 μM) | Pyrimethamine (10 μM) |

### Bidirectional transcellular transport assays (MDR1 / BCRP)

LLC-PK1 cells, MDCKII cells, and L-MDR1, M-BCRP transfected cells (obtained from Dr. A. Schinkel, The Netherlands Cancer Institute [Amsterdam, The Netherlands] and used under a license agreement) were cultivated at 37°C in a humidified 5% $CO_2$ cell culture incubator; preparation and characterization of the cell lines have been reported elsewhere (Schwab et al., 2003). The experiments were performed on a Tecan automated liquid handling system using 96-insert plates. The medium was removed from apical and basolateral compartments and replaced on the receiver side by culture medium without phenol red, with or without inhibitor. The transcellular transport measurement was initiated by adding the test compound dissolved in culture medium together with the extracellular marker (lucifer yellow) to the donor side. The MDR1 inhibitor (zosuquidar [1 μM] or test compound) was added to both sides. The transport experiment was performed in both directions in triplicate. The plates containing the inserts were incubated at 37°C and 5% $CO_2$ with continuous shaking (100 rpm). Samples were taken from the donor and the opposite (acceptor) side after 3 h incubation. Concentrations of substrate in both compartments were determined by scintillation counting for radioactive compounds (digoxin, quinidine and radiolabeled test compound) or by LC-MS/MS for the test compound. The extracellular marker (lucifer yellow) was quantified using a Multimode Plate Reader ENSPIRE from Perkin Elmer at 430/535 nm (Ex/Em). Triplicate inserts were used for each condition. Experiments showing lucifer yellow permeation superior to 1%/h were rejected.

## Translating *in vitro-in vivo-in silico* data to first-in-human trials

### Physiologically based pharmacokinetic (PBPK) model

PBPK model of risdiplam was developed using the population-based PBPK software Simcyp (Simcyp Ltd, a Certara company, Sheffield, UK; version 15). Graphics were created using R version 3.2.3 with RStudio version 0.99.489. Absorption of risdiplam was modeled by integrating physicochemical properties, physiology and anatomy of the gastrointestinal tract using the ADAM (Advanced Dissolution Absorption and Metabolism) model for oral solution of Simcyp. A stable supersaturation status of risdiplam was shown independent of pH and concentration of bile salts *in vitro* and therefore formation of precipitation was not considered in the absorption modeling. Volume of distribution (Vss) was described with Kp values which was measured in a distribution study in cynomolgus monkeys (Poirier et al., 2018) and available for 8 out of 12 organs considered

in Simcyp for distribution. Estimated values according to Rodgers et al. (Rodgers et al., 2005) were used for the remaining organs.

The clearance was predicted based on the intrinsic hepatic clearance determined in a long-term incubation with HepatoPac®, and the relative turnover of risdiplam in the incubations with liver, intestine and kidney microsomes. The extent of the first pass extraction in the gut was predicted based on the determined relative turnover. The model was evaluated by comparing simulated plasma concentration time profiles of risdiplam with those observed in healthy male individuals who received a single dose of risdiplam 0.6, 2, 6 or 18 mg [Sturm et al. (2018)]. The simulation was performed using the default healthy volunteer model after matching the age, body weight and height distribution as the actual study population, followed by the actual study design and repeated 10 times. The observed renal clearance and the results of the itraconazole drug-drug interaction (DDI) investigation in the SAD study [Sturm et al. (2018)] were used to further expand the clearance model.

### Population PK (PPK) modeling for healthy adults

A PPK model was constructed on 429 observations collected in 26 healthy male individuals receiving a single dose of 0.6 to 18 mg of risdiplam in the SAD study (Sturm et al., 2018). NONMEM software version 7.2.0 (ICON PLC, Dublin, Ireland) was used for the modeling.

# Results

## Low *in vitro* turnover of risdiplam warranted early confirmation of MIST-relevant metabolites in human plasma samples

**Figure S1: Proposed main metabolic pathway for $^{14}$C-risdiplam in humans**

Overview of main metabolite structures of risdiplam identified *in vitro* and in healthy male individuals following a single 18 mg oral dose. All observed *in vivo* circulating metabolites and those that accounted individually for more than 1.5% of the dose in excreta are annotated in bold. (Italics *in vitro* observations only). Apart from M1 most observed metabolite structures are the result of multiple metabolic reactions mainly involving oxidative metabolism at the cyclopropyl and piperazine moiety. When metabolite structures were confirmed by nuclear magnetic resonance spectroscopy they are shown as definitive structures (M1, M2, M3). Others are shown as Markush structures indicating the part of risdiplam metabolized and the corresponding change in the elemental formula relative to risdiplam.

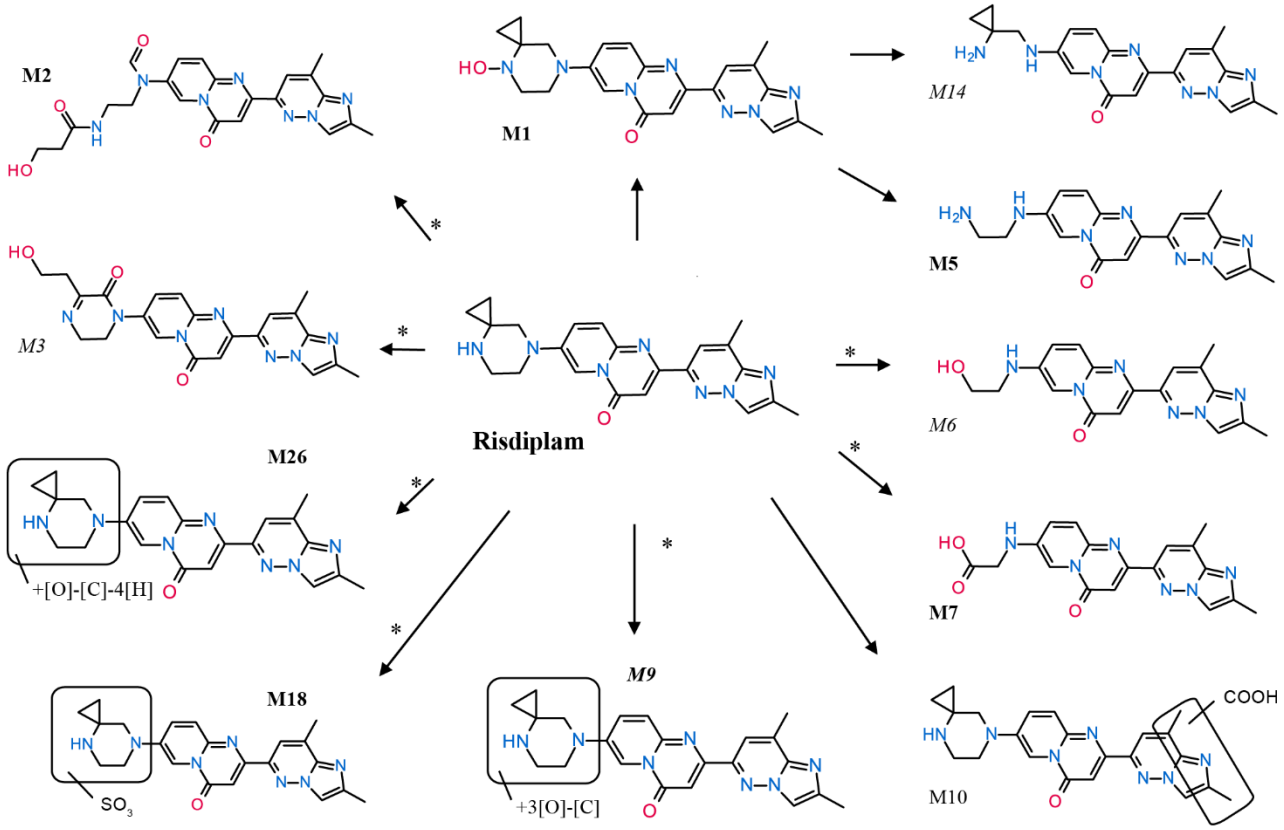


*Several, initial and intermediate metabolite structures which would be required to describe the sequential metabolism of risdiplam were not observed and remain elusive.

## hADME study

### *Demographics and safety*

The mean age of the six healthy male individuals enrolled in NCT03036501 was 53.2 years (range: 41–62 years) at baseline and all individuals completed the study. A total of 18 AEs were reported, and all six

individuals experienced at least one AE. The most frequently reported AE was dry skin (three individuals). There were no AEs of severe intensity were reported, and no individual was withdrawn from the study as a result of an AE. There were no clinically significant abnormalities in laboratory assessments, ophthalmology tests and ECG.

*Recovery of total drug-related material in urine and feces*

An overview of the cumulative recovery of radioactivity in the excreta of six healthy individuals following oral administration of 18 mg of [$^{12}$C/$^{14}$C]-risdiplam is shown in **Table S2**. An average of 81.4% (range 60.3% to 89.6%) of radioactivity was recovered within 840-h study observation period. Most of the radioactivity (>80% of the dose) was recovered within the first 168 h after drug administration. The pattern of radioactive elimination was broadly similar between the individuals (15.6 to 33.7% and 44.7% to 62.1% of the dose recovered in urine and feces, respectively). One individual had a substantially lower recovery (60.3%) compared with the other individuals, which may be due to incomplete sample collection. With this individual excluded, the resulting mean total recovery of the administered dose was 85.6% for the remaining five individuals.

*Drug-related material in human plasma*

In plasma, unchanged risdiplam was the major component accounting for 83% of drug-related material in circulation (percent of $AUC_{0\text{-}48h}$). The metabolite M1 (*N*-oxidation of risdiplam) was identified as the major circulating metabolite and represented 14% of drug-related $AUC_{0\text{-}48h}$. Four additional low-level metabolites (M2, M7, M9 and M26) were observed from the biotransformation of the piperazine moiety. Through protein precipitation, extraction of drug-related material from human plasma was considered near complete with ≥80% recovery of all radioactivity in each sample. Through HPLC methodologies, the recovery in plasma was ≥90% for each sample. Relative to the AUC of the total drug-related material in plasma, no individual metabolite accounted for >3.3%. The metabolic profiles of total radioactivity in pooled plasma samples were acquired across all six individuals at 1, 4.5, 12, 24 and 48 h post-dose. Plasma time profile and representative radiochromatograms of risdiplam and metabolites are depicted in **Figure S2** and **S3** and individual metabolite abundance in plasma listed in **Table S3**.

**Table S2: Overall cumulative recovery of [$^{14}$C]-radioactivity in urine and feces and total excretion (percentage of dose administered) by individuals with summary statistics.**

| Subject | Cumulative radioactivity recovered (% of dose) | | |
|---|---|---|---|
| | Urine | Feces | Total |
| 1 | 15.6 | 44.7 | 60.3 |
| 2 | 27.5 | 62.1 | 89.6 |
| 3 | 31.8 | 53.3 | 85.1 |
| 4 | 27.3 | 61.4 | 88.7 |
| 5 | 33.0 | 52.3 | 85.3 |
| 6 | 33.7 | 45.6 | 79.3 |
| **Mean** | **28.2** | **53.2** | **81.4** |
| CV% | 23.9 | 14.0 | 13.4 |
| Min-Max | 15.6–33.7 | 44.7–62.1 | 60.3–89.6 |

CV = coefficient of variation; Min = minimum; Max = maximum.

**Table S3. Metabolite profiles in human plasma after oral administration of risdiplam.**

| Retention time (mins) | Metabolite | Abundance of plasma metabolites | | | | | |
|---|---|---|---|---|---|---|---|
| | | % of total radioactivity in chromatogram | | | | | % of total radioactive AUC‡ |
| | | ng eq/mL* | | | | | ng eq•h/mL† |
| | | 6 individual pool (1001, 1002, 1003, 1004, 1005, and 1006) | | | | | |
| | | 1h | 4.5h | 12 h | 24h | 48h | 0-48h |
| 18.8 | risdiplam | 93.3 | 87.4 | 86.7 | 79.6 | 80.1 | 83.2 |
| | | 65.0 | 72.7 | 52.1 | 45.9 | 37.1 | 2330 |
| 34.3 | M1 | 4.58 | 8.59 | 11.8 | 17.1 | 17.9 | 14.0 |
| | | 3.19 | 7.16 | 7.12 | 9.84 | 8.29 | 393 |
| 15.5 | M2+M7 | 2.13 | 2.15 | nd | nd | nd | 0.471 |
| | | 1.48 | 1.79 | nd | nd | nd | 13.2 |
| 21.9 | M9 | nd | 0.657 | nd | nd | nd | 0.108 |
| | | nd | 0.548 | nd | nd | nd | 3.02 |
| 27.3 | M26 | nd | 1.24 | 1.52 | 3.28 | 1.95 | 2.12 |
| | | nd | 1.03 | 0.918 | 1.89 | 0.902 | 59.4 |
| Total (%) | | 100 | 100 | 100 | 100 | 100 | 100 |
| Total ng eq (•h)/mL | | 34.8 | 267 | 538 | 707 | 1250 | 2800 |

nd – not detected in the radiochromatogram

*ng eq/mL for individual components = ([% of total radioactivity in chromatogram at time-point] x [total ng eq/mL at time-point]) ÷ 100.

†ng eq·h/mL for individual components are calculated from the ng eq/mL values using the linear trapezoidal method.

‡% of total radioactive AUC for each component = ([ng eq·h/mL for individual component] ÷ [total ng eq·h/mL]) x 100.

**Figure S2. Representative metabolite radiochromatograms for plasma pooled from six individuals following a single oral dose of [$^{14}$C]risdiplam at 1, 4.5, 24 and 48 h (bottom) post-dose. Signals that were assigned to metabolite structures have been labeled.**

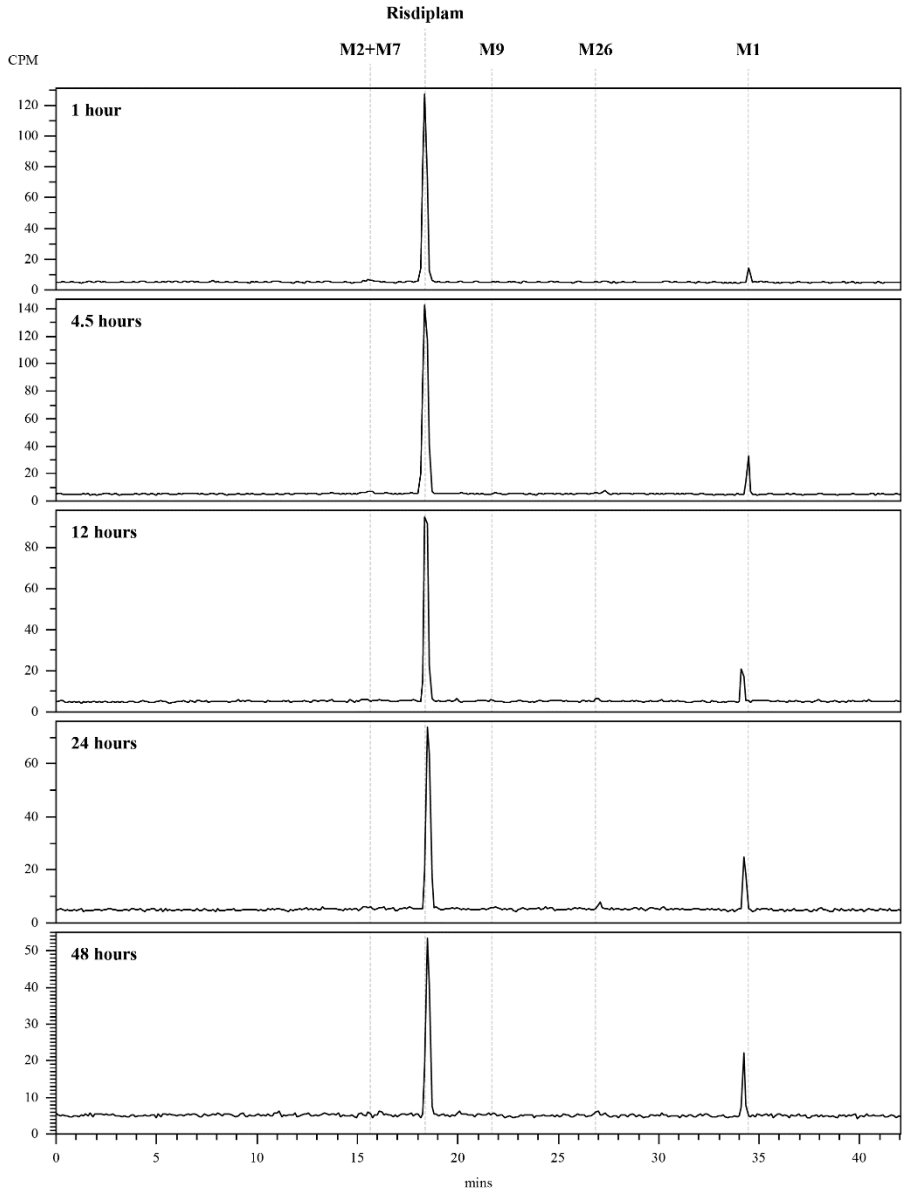


*Metabolic profile of risdiplam in excreta*

The total recovery indicated that the duration of sample collection for feces and urine was adequate to characterize the excretion balance of risdiplam. Approximately 53.2% (range 44.7% to 62.1%) of the [$^{14}$C]-risdiplam dose was recovered through the feces. The main drug-related component in feces was the parent compound, which accounted for 14% of the dose (0-168 h). The metabolites M5, M7 (both resulting from biotransformation of the piperazine moiety) and M10 (carboxylic acid metabolite) were the most abundant components accounting for 3.0, 4.1 and 2.2% of the dose, respectively. In addition, several other low-level metabolites (>30) metabolites with individual contributions below 1.5% of the dose were observed.

The recovery of drug-related material from the human feces pool samples after sample preparation was 94.6%; HPLC recovery was 92%.

Approximately 28% (range 15.6% to 33.7%) of the recovered dose administered was found in urine. Risdiplam was the main drug-related component which accounted for 7.7% of the dose. The most abundant metabolite was M7, accounting for 1.8% of the dose. Additional low-level metabolites were observed in urine (mainly involving biotransformation of the piperazine moiety), but no single component accounted for more than 1.0% of the dose. The HPLC recovery of risdiplam in urine after sample preparation was 99%.

Representative radiochromatograph profiles of feces and urine are given in **Figure S3**.

**Figure S3. Representative metabolite radiochromatograms for feces and urine (pool of 6 individuals 0–168 h) after oral administration (18 mg) of [$^{14}$C] risdiplam.**

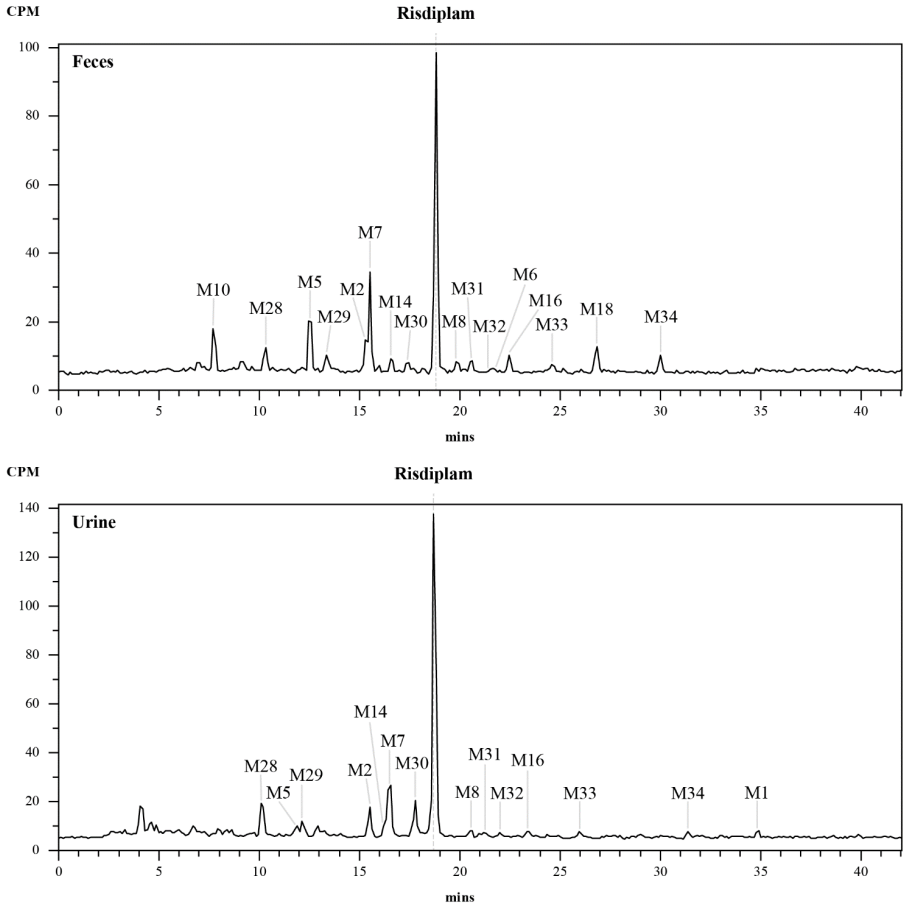


## PK of a single oral dose of [$^{14}$C/$^{12}$C]-risdiplam

The plasma time profiles for risdiplam and total radioactivity in plasma and blood are shown in **Figure S4a** and **S4b** with the PK parameter summarized in **Table S4**. The median times to reach $C_{max}$ were observed at 3 and 3.5 h for plasma and blood, respectively. Based on radioactivity detection the mean $C_{max}$ in plasma and blood were 84.7 and 71.7 ng/mL, respectively. For $^{12}$C-risdiplam (LC-MS) the geometric means (geo mean CV%) $C_{max}$ were determined at 70 ng/mL (17.0%) in plasma. After reaching $C_{max}$ $^{12}$C-risdiplam concentrations in plasma declined with an apparent terminal elimination half-life of 78.8 h (26.5%). The $AUC_{inf}$ in plasma was determined at 2990 h.ng/mL (31.7%). The time course of [$^{14}$C]-radioactivity in plasma and blood and that of

$^{12}$C-risdiplam in plasma were similar over the first 24 h after administration. However, the concentration versus time profiles diverged thereafter, demonstrating that the time course of drug-related [$^{14}$C]-radioactivity in plasma was associated with longer half-lives compared with risdiplam.

**Table S4. Summary of [$^{14C}$]-radioactivity PK parameters in plasma and blood following single oral dose administration of 18 mg [$^{14}$C/$^{12}$C]-risdiplam.**

| [$^{14}$C]-radioactivity | $T_{max}$ (h) | $C_{max}$ (ng/mL) | $AUC_{inf}$ (h • ng/mL) | $AUC_{last}$ (h • ng/mL) | HL (h) |
|---|---|---|---|---|---|
| **Plasma (N=6)** | 3.02 (1.00 – 4.50) | 84.7 (21.6%) | ND | 12200 (37.6%) | ND |
| **Blood (N=6)** | 3.50 (2.00 – 4.50) | 71.7 (17.1%) | ND | 3950 (49.2%) | ND |
| **[$^{12}$C]-risdiplam** | | | | | |
| **Plasma (N=6)** | 2.00 (2.00 – 4.00) | 70.0 (17.0%) | 2990 (31.7%) | ND | 78.8 (26.5%) |

Median (min, max) for Tmax, geometric mean (geo mean CV%) otherwise. ND: not determined.

**Figure S4a. Mean (+ SD) [$^{14}$C]-radioactivity concentration versus time profiles in plasma and blood (linear scale).**

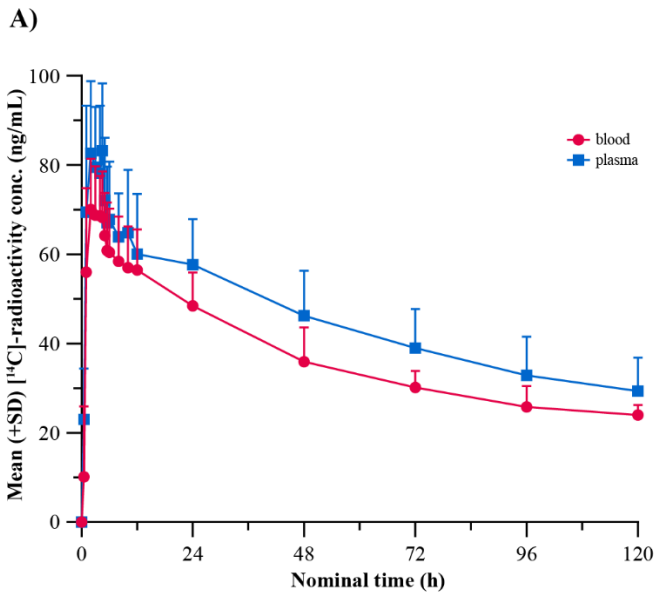


Conc, concentration; SD, standard deviation.

**Figure S4b. Mean (+ SD) [$^{12}$C]-risdiplam plasma concentration versus time profile (linear scale).**

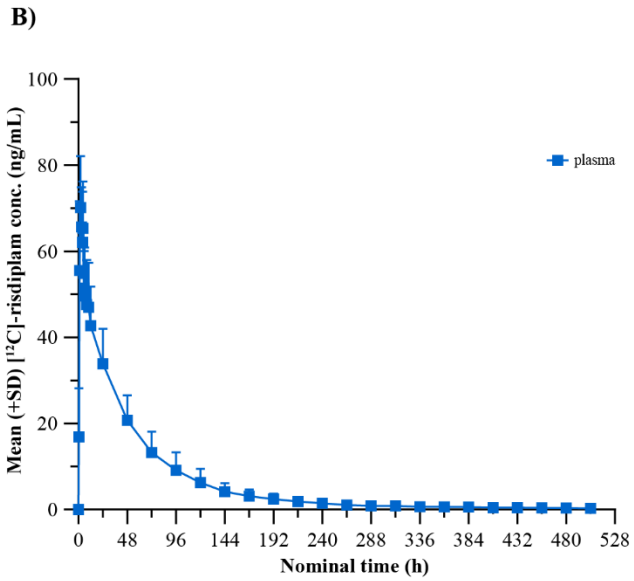


Conc, concentration; SD, standard deviation.

## Investigating the combination of CYP and FMO contributions to risdiplam metabolism and implications for victim DDIs

The percent turnover of radio-labeled risdiplam was assessed through recombinantly expressed CYP and FMO enzymes after 1 h of incubation **(Table S5)**. High relative rates of oxidative metabolism by kidney microsomes highlighted the possibility for FMO1 involvement. Investigation of the $^{14}$C-risdiplam metabolism by recombinantly expressed CYP and FMO enzymes showed that risdiplam can be metabolized by both FMO1 and FMO3 as well as by CYPs 1A1, 3A4, and 3A7.

**Table S5. Turnover of 10 µM $^{14}$C-labeled risdiplam by recombinantly expressed CYP and FMO enzymes after 1 h of incubation.**

| Test system | %turnover risdiplam |
|---|---|
| HLM | 24 |
| Human kidney microsomes | 9 |
| Human intestinal microsomes | 2 |
| CYP1A1 | 6.9 |
| CYP1A2 | ND |
| CYP2B6 | ND |
| CYP2C8 | ND |
| CYP2C9 | ND |
| CYP2C19 | ND |
| CYP2D6 | ND |
| CYP3A4 | 8.3 |
| CYP3A5 | 3.0 |
| CYP3A7 | 7.1 |
| FMO1 | 72.3 |
| FMO3 | 62.4 |

Incubation with the CYP3A-selective inhibitor (ketoconazole) and the FMO inhibitor (methimazole) showed that both CYP3A and FMO enzymes contributed substantially to risdiplam metabolism by HLM (**Table S6**). Incubation with CYP1A inhibitor α-naphthoflavone indicated that CYP1A enzymes did not contribute significantly to pooled HLM metabolism. The contribution of CYP2J2 was not explored in this experiment due to lack of a selective inhibitor. Overall *in vitro* data indicated that FMO3, CYP3A4 and other CYP enzymes contributed to hepatic metabolism and that FMO1 would be expected to contribute to extrahepatic metabolism in the kidney.

**Table S6: Activity of pooled HLM in metabolism of 1 µM risdiplam to metabolites M1, M2 and M5 in the presence of chemical inhibitors.**

| Inhibitor/enzyme | M1 | M2 | M5 |
|---|---|---|---|
| CYP1A1/1A2: a-NF | 102 ±4 | 100 ±4 | 97 ±7 |
| CYP2B6: Ticlopidine | 102 ±6 | 94 ±3 | 95 ±7 |
| CYP2C8: Montelukast | 86 ±2 | **75 ±8** | **79 ±9** |
| CYP2C9: Sulfaphenazole | 90 ±2 | 93 ±17 | 97 ±20 |
| CYP2C19: Benzyphenobarbital | 98 ±9 | 100 ±5 | 103 ±10 |
| CYP2D6: Quinidine | 82 ±14 | 85 ±11 | 89 ±1 |
| CYP3A4/5: Ketoconazole | **38 ±3** | **77 ±9** | **72 ±10** |
| FMO3: Methimazole | **54 ±7** | 83 ±4 | **78 ±3** |

Values indicating more than 15% inhibition effect shown in bold text.

Microsomes were tested at a concentration of 1 mg/mL, recombinantly expressed CYPs at a concentration of 200 pmol/mL and FMO enzymes at a SF9 membrane protein concentration of 0.25 mg/mL. ND: not detected above background. Limits of quantitation 3% for recombinant enzyme experiments, 1% for liver microsomes.

## Translating *in vitro-in vivo-in silico* data to first-in-human trials

### Population PK modeling

The best structural model fitted to the data is a 3-compartmental catenary model with first-order elimination for disposition and 2-transit compartments for absorption as summarized in **Table S7**. For the three individuals who received 6 mg of risdiplam after a high-fat breakfast a separate transit rate constant for absorption was estimated to describe the influence of fed state on absorption. The goodness of fit plots and visual predictive check shows that the PPK model adequately describes risdiplam PK after single dose of 0.6 to 18 mg of risdiplam in these 26 healthy male individuals (**Figure S5**).

**Table S7. Summary of the PPK model parameters.**

| Parameter | Unit | Estimate | RSE (%) |
|---|---|---|---|
| **Fixed Effects** | | | |
| CL/F | L/hr | 5.68 | 6.90 |
| $V_c$/F | L | 194 | 8.40 |
| Ka (fasted) | $hr^{-1}$ | 3.21 | 11.1 |
| Ka (fed) | $hr^{-1}$ | 2.03 | 41.0 |
| $Q_c$/F | L/hr | 17.0 | 41.7 |
| $V_{p1}$/F | L | 86.9 | 15.5 |
| $Q_p$/F | L/hr | 0.761 | 11.8 |
| $V_{p2}$/F | L | 108 | 14.4 |
| **Random Effects BSV** | | | |
| CL/F | CV% | 17.6 | 28.2 |
| $V_c$/F | CV% | 19.6 | 31.5 |
| Ka | CV% | 32.4 | 23.7 |
| $V_{p1}$/F | CV% | 24.2 | 44.3 |
| **Residual Error Model** | | | |
| $\sigma_1$ (proportional) | % | 12.0 | 3.00 |

Ka: transit rate constant, CL/F: apparent clearance, $V_c$/F: apparent central volume of distribution, $Q_c$/F: apparent inter-compartmental clearance (central), $V_{p1}$/F: apparent peripheral volume of distribution 1, $Q_p$/F: apparent inter-compartmental clearance (peripheral), $V_{p2}$/F: apparent peripheral volume of distribution 2,RSE: relative standard error, BSV: between subject variability.

**Figure S5. Goodness of fit plots of the basic PPK model.**

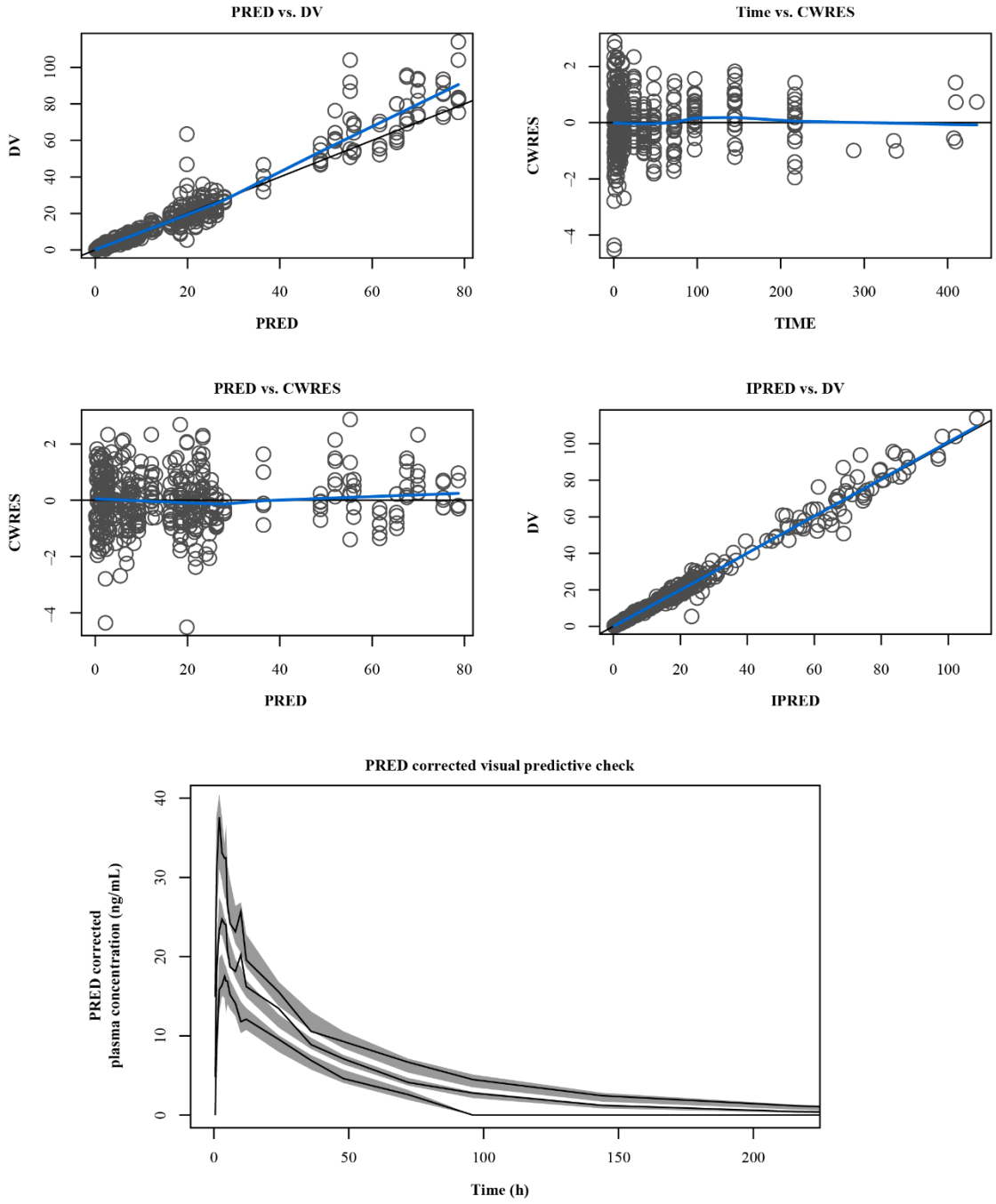


Identity line (black) and smooth (blue) are shown. PRED: population prediction, IPRED: individual prediction, CWRES: conditional weighted residual, IWRES: individual weighted residual. PRED corrected visual predictive check shows 5$^{th}$, median and 95$^{th}$ percentiles of the observations (solid lines) compared with the respective 90% prediction intervals (grey shade).

## DDIs risk profile – clinical relevance of CYP3A TDI and emerging transporters

**Table S8** summarizes the direct inhibition, TDI and induction parameters of risdiplam and M1 on CYP enzymes. Risdiplam and M1 did not show direct inhibition of major CYP enzymes except for CYP3A concentrations of up to 12.5 μM and 10 μM, respectively, which are greater than the $C_{max}$ values (184 ng/mL for patients with infantile-onset SMA and 148 ng/mL for patients with later-onset SMA) after oral administration at the therapeutic dose of risdiplam, indicating no clinically relevant direct inhibition on CYP substrates. *In vitro* TDI parameters of risdiplam and M1 on CYP3A were measured as $K_I$ = 13 μM and $k_{inact}$ = 0.065 $min^{-1}$; and $K_I$ = 13.7 μM, $k_{inact}$= 0.063 $min^{-1}$, respectively.

No significant increase in the mRNA level of CYP1A2, 2B6, 2C8, 2C9, 2C19 and 3A4 relative to the vehicle control was observed after incubation of risdiplam and M1 up to 1 μM with primary human hepatocytes.

**Table S8: *In vitro* assessment of DDI of risdiplam and M1 with human drug-metabolizing enzymes and transport proteins**

| | | Perpetrator | |
|---|---|---|---|
| | | Risdiplam | M1 |
| Drug-metabolizing enzymes | CYP reversible and TDI (1A2, 2B6, 2C8, 2C9, 2C19, and 2D6) | No signal up to 12.5 μM | No signal up to 10 μM |
| | CYP3A4 reversible inhibition | $IC_{50}$ = 11 μM | No signal up to 10 μM |
| | CYP3A4 TDI | $K_I$ = 13 μM, $k_{inact}$ = 0.065 $min^{-1}$ | $K_I$ = 13.7 μM, $k_{inact}$ = 0.063 $min^{-1}$ |
| | CYP induction (1A2, 2B6, 2C8, 2C9, 2C19, and 3A4) | No signal up to 1 μM | No signal up to 1 μM |
| Transport proteins | MDR1 | No signal up to 50 μM | $IC_{50} \geq$ 10 μM[a] |
| | BCRP | $IC_{50} \geq$ 20 μM [a] | $IC_{50}$ = 2.3 μM |
| | OATP1B1 | No signal up to 50 μM | No signal up to 50 μM |
| | OATP1B3 | No signal up to 50 μM | No signal up to 50 μM |
| | OAT1 | No signal up to 50 μM | $IC_{50} \geq$ 20 μM[a] |
| | OAT3 | No signal up to 50 μM | No signal up to 20 μM |
| | OCT2 | $IC_{50}$ = 8.7 μM | $IC_{50} \geq$ 20 μM [a] |
| | MATE1<br>MATE2-K | $IC_{50}$ = 0.15 μM<br>$IC_{50}$ = 0.09 μM | $IC_{50}$ = 14.8 μM<br>$IC_{50} \geq$ 20 μM[a] |

[a]Less than 50% inhibition at the maximum soluble concentration in the *in vitro* system.

# References

Ballard TE, Kratochwil NA, Cox LM, Moen MA, Klammers F, Ekiciler A, Goetschi A, and Walter I (2020) Simplifying the Execution of HepatoPac MetID Experiments: Metabolite Profile and Intrinsic Clearance Comparisons. *Drug Metab Dispos***:**DMD-AR-2020-000013.

Khetani SR and Bhatia SN (2008) Microscale culture of human liver cells for drug development. *Nature Biotechnology* **26:**120-126.

Kratochwil NA, Meille C, Fowler S, Klammers F, Ekiciler A, Molitor B, Simon S, Walter I, McGinnis C, Walther J, et al. (2017) Metabolic Profiling of Human Long-Term Liver Models and Hepatic Clearance Predictions from In Vitro Data Using Nonlinear Mixed-Effects Modeling. *AAPS J* **19:**534-550.

Poirier A, Weetall M, Heinig K, Bucheli F, Schoenlein K, Alsenz J, Bassett S, Ullah M, Senn C, Ratni H, et al. (2018) Risdiplam distributes and increases SMN protein in both the central nervous system and peripheral organs. *Pharmacol Res Perspect* **6:**e00447.

Rodgers T, Leahy D, and Rowland M (2005) Physiologically Based Pharmacokinetic Modeling 1: Predicting the Tissue Distribution of Moderate-to-Strong Bases. *J Pharm Sci* **94:**1259-1276.

Schwab D, Fischer H, Tabatabaei A, Poli S, and Huwyler J (2003) Comparison of in vitro P-glycoprotein screening assays: recommendations for their use in drug discovery. *J Med Chem* **46:**1716-1725.

Sturm S, Gunther A, Jaber B, Jordan P, Al Kotbi N, Parkar N, Cleary Y, Frances N, Bergauer T, Heinig K, et al. (2018) A phase 1 healthy male volunteer single escalating dose study of the pharmacokinetics and pharmacodynamics of risdiplam (RG7916, RO7034067), a SMN2 splicing modifier. *Br J Clin Pharmacol* **85:**181-193.